FINITE-AMPLITUDE WAVES IN IMPERFECT CAVITIES

Roger Ronald DeVall

NAVAL POSTGRADUATE SCHOOL
Monterey, California

THESIS

FINITE-AMPLITUDE WAVES
IN
IMPERFECT CAVITIES

by

Roger Ronald DeVall

Advisor: J. V. Sanders

December 1973

Approved for public release; distribution unlimited.

Finite-Amplitude Waves in Imperfect Cavities

by

Roger Ronald DeVall
Lieutenant, United States Navy
B.S., California State University at Los Angeles, 1965

Submitted in partial fulfillment of the
requirements for the degree of

MASTER OF SCIENCE IN ENGINEERING ACOUSTICS

from the

NAVAL POSTGRADUATE SCHOOL
December 1973

ABSTRACT

Finite-amplitude standing waves in air at ambient temperatures contained within a detunable, rigid-walled rectangular cavity were experimentally investigated. The pressure waveforms resulting from excitations in the vicinity of the resonances of the 100 and 010 modes were analyzed for harmonic content at three different cavity configurations. Similarly, waveforms of the 110 and 210 modes were analyzed for four different cavity configurations. These results were compared to the predictions of a theory of Coppens and Sanders wherein the resonance frequencies and quality factors of all modes were experimentally determined from infinitesimal-amplitude measurements. It was found that in the case of nearly degenerate modes, coupling within the cavity allowed for the excitation of modes belonging to families other than that containing the driven mode. This feature is absent from the theory in its present form.

TABLE OF CONTENTS

I. INTRODUCTION 4

II. BACKGROUND AND THEORY 5

III. EXPERIMENTAL CONSIDERATIONS 9

A. APPARATUS 9

B. MICROPHONE OUTPUT AND STRENGTH PARAMETER . . . 13

C. FREQUENCY PARAMETER 14

D. CAVITY ISOLATION 14

IV. DATA TAKING PROCEDURES 15

A. PRERUN PROCEDURES 15

B. INFINITESIMAL AMPLITUDE ANALYSIS 16

C. FINITE AMPLITUDE ANALYSIS 18

V. RESULTS 20

VI. CONCLUSIONS 51

BIBLIOGRAPHY 59

INITIAL DISTRIBUTION LIST 60

FORM DD 1473 61

I. INTRODUCTION

The purpose of this research is to investigate finite-amplitude standing waves in air at ambient temperatures in imperfect rigid walled cavities for comparison with the theory of Coppens and Sanders [1]. This investigation was a continuation of the experimental works of Lane [2], with modifications to take into account the non-ideal nature of the cavity.

II. BACKGROUND AND THEORY

A plane elastic wave traveling in a non-dissipative medium will change wave form as predicted by hydrodynamic equations. If the problem is extended to absorptive media, only waves of relatively high amplitude will change waveforms. Thus, a finite-amplitude wave is a solution of the nonlinear wave equation that describes the real life environment that confronts large amplitude acoustic waves. This finite-amplitude wave requires second order terms, or higher, to describe the waveform.

The study of finite-amplitude effects in standing waves is the logical extension of earlier studies dealing with traveling waves [3, 4, 5, 6, and 7]. The theory of Coppens and Sanders [1] deals with finite-amplitude standing waves in rigid walled cavities. It is an extension of the Keck-Beyer [8] perturbation approach which makes use of perturbation methods and Fourier series representations of the waveform. Initially, the theory included wall losses as predicted by Rayleigh-Kirchoff theory [9]. This approach was investigated by Ruff [10] to the tenth harmonic, at which the mathematics became divergent. Coppens [11] expanded the theory and used a Fourier decomposition technique that was experimentally investigated in tubes by Beech [12] and Winn [13]. The tubes investigated did not behave in a manner predicted by Rayleigh-Kirchoff loss mechanisms. The theory was revised to include empirically determined losses which was subsequently investigated by Lane [2]. Lane

investigated standing waves in a rigid rectangular cavity and found that the theoretical model successfully predicted the major features of the harmonic content for finite-amplitude standing waves.

The theory of Coppens and Sanders developes a one-dimensional, non-linear wave equation with dissipative terms which correspond to those encountered in the description of plane standing waves in a rigid-walled cavity. The wave equation is then Fourier decomposed to take the form

$$\sum_{n=1}^{\infty} \left(\frac{\partial^2}{\partial x^2} - \frac{1}{C_o^2} \frac{\partial^2}{\partial t^2} + D_n\right) \frac{\partial \xi_n}{\partial x} = b \frac{\partial^2}{\partial x^2} \left(\frac{\partial \xi}{\partial x}\right)^2 \qquad (1)$$

where

$$D_n = \delta_1 \left(\frac{1}{\omega_{1r} n^{3/2}} \frac{\partial^3}{\partial x^2 \partial t} - \frac{1}{n^{1/2}} \frac{\partial^2}{\partial x^2}\right)$$

and contains a dispersive term and a dissipative term, both based on the Rayleigh-Kirchoff theory of wall losses [9], and

$\delta_1 = 1/Q_1$

ξ_n = particle displacement due to n^{th} harmonic

$\xi = \Sigma_n \xi_n$

$b = (1 + C_p/C_v)/2$

C_p = specific heat of medium at constant pressure

C_v = specific heat of medium at constant volume

ω_{1r} = frequency (angular) of fundamental resonance

$$Q_1 = \frac{\omega_{1r}}{\omega_{1+} - \omega_{1-}}$$

$\omega_{1+} - \omega_{1-}$ is the difference of the half power frequencies above and below the fundamental.

Equation 1 can be reformulated [2] to introduce the actual cavity resonances and generalized to include an arbitrary, empirical absorption coefficient for each mode. The result is

$$\sum_{n=1}^{\infty} K_n^2 \left[\frac{2\Delta\omega_n}{\omega_{nr}} - \frac{1}{n\omega} \frac{1}{Q_n} \frac{\partial}{\partial t} \right] \frac{\partial \xi_n}{\partial x} = b \frac{\partial^2}{\partial x^2} \left(\frac{\partial \xi}{\partial x} \right)^2$$

where

ω_{nr} = resonance frequency of the n^{th} overtone

$K_n = \frac{4\pi}{nL}$ such that pressure antinodes exist at x = 0 and at x = L

$\Delta\omega_n = n\omega - \omega_{nr}$

ω = frequency at which system is being driven (near ω_{1r})

$Q_n = \frac{\omega_{nr}}{\omega_{n+} - \omega_{n-}}$

ω_{n+} and ω_{n-} are the half power frequencies above and below ω_{nr}

The acoustic pressure is the

$$\frac{\partial \xi}{\partial x} = \frac{p}{\rho_o C_o^2} = M \sum_{n=1}^{\infty} R_n \cos K_n(L-x) \cos n(\omega t + \phi_n)$$

p = acoustic pressure

ρ_o = density of medium

C_o = thermodynamic speed of sound in medium

M = mach number = $p_1/\rho_o C_o^2$

p_1 = peak pressure of fundamental component of wave

R_n = Fourier coefficient of n^{th} harmonic component, normalized such that $R_1 = 1$

and

ϕ_n = phase angle of n^{th} harmonic component, where $\phi_1 = 0$.

This equation is then manipulated into a general, time-independent form which, when evaluated at the rigid boundaries of the cavity, can be further simplified to produce the following form amenable to computer calculation:

$$H_n R_n \cos(\phi_n - \theta_n) = MbQ_1 \; 1/2 \left\{ 1/2 \sum_{j=1}^{n=1} R_j R_{n-j} \cos(\phi_j + \phi_{n-j}) - \sum_{j=1}^{\infty} R_{n+j} R_j \cos(\phi_{n+j} - \phi_j) \right\}$$

and a similar form with "sin" in place of "cos",

where

$$H_n = \sqrt{\left(\frac{2\Delta\omega_n}{\omega_{nr}} Q_1\right)^2 + \left(\frac{Q_1}{Q_n}\right)^2}$$

and

$$\tan \theta_n = \frac{2\Delta\omega_n Q_1/\omega_{nr}}{Q_1/Q_n} .$$

The above equations show the importance of knowing the Q_n and ω_{nr} of the system for input to the computer program. For convenience, a quantity, E_n, is defined to indicate the position of ω_{nr} relative to the classical harmonic frequencies, $n\omega_{1r}$.

$$E_n = \frac{\omega_{nr} - n\omega_{1r}}{n\omega_{1r}}$$

The values of Q_n and E_n are directly determined from the infinitesimal-amplitude analysis of the cavity and are the input quantities for the computer calculations.

III. EXPERIMENTAL CONSIDERATIONS

A. APPARATUS

The rectangular cavity is shown in Figure 1. It was constructed with 0.985 inch thick aluminum plates, milled and screwed together to provide tight, right angle joints. The joints were sealed with thin layers of high-vacuum silicon grease which was applied to all ajoining surfaces prior to assembly. The interior dimensions were 6.97cm by 20.96 cm by 25.12cm. The theoretically predicted modes assuming an ideal rectangular cavity are shown in Table 1. The accesses were provided to the cavity for the piston and microphone. These were positioned at opposite corners of the cavity.

A block diagram of the experimental apparatus is shown in Figure 2. Acoustic waves were generated within the cavity by a plane-faced piston. The piston gained access to the interior of the cavity by way of the large orifice. It was fitted with one O-ring which was lubricated and further sealed with high vacuum silicon grease to provide an airtight fit. An Endeveco Model 2215 accelerometer was mounted on the inner face of the piston which enabled the piston motion to be monitored on a Hewlett Packard Model 400D voltmeter, a Fairchild Model 766H dual trace oscilloscope, and a Hewlett Packard 302A wave analyzer. The piston was attached to a MB Electronics Model 2120MB power amplifiers operating in parallel. The frequency and power level of the piston were controlled by a General Radio 1161-A coherent decade frequency synthesizer. The

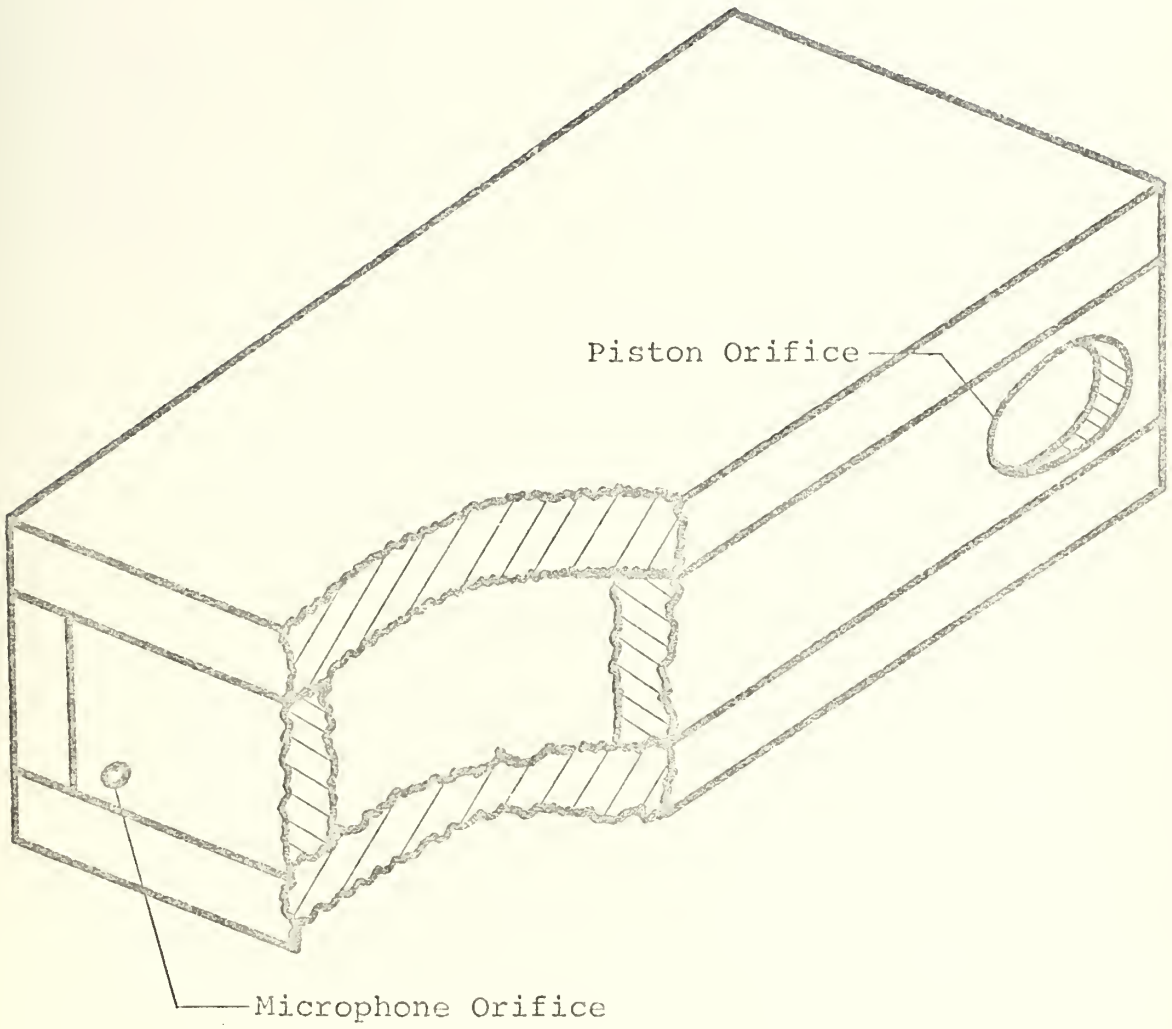

FIGURE 1. Rigid Walled Cavity

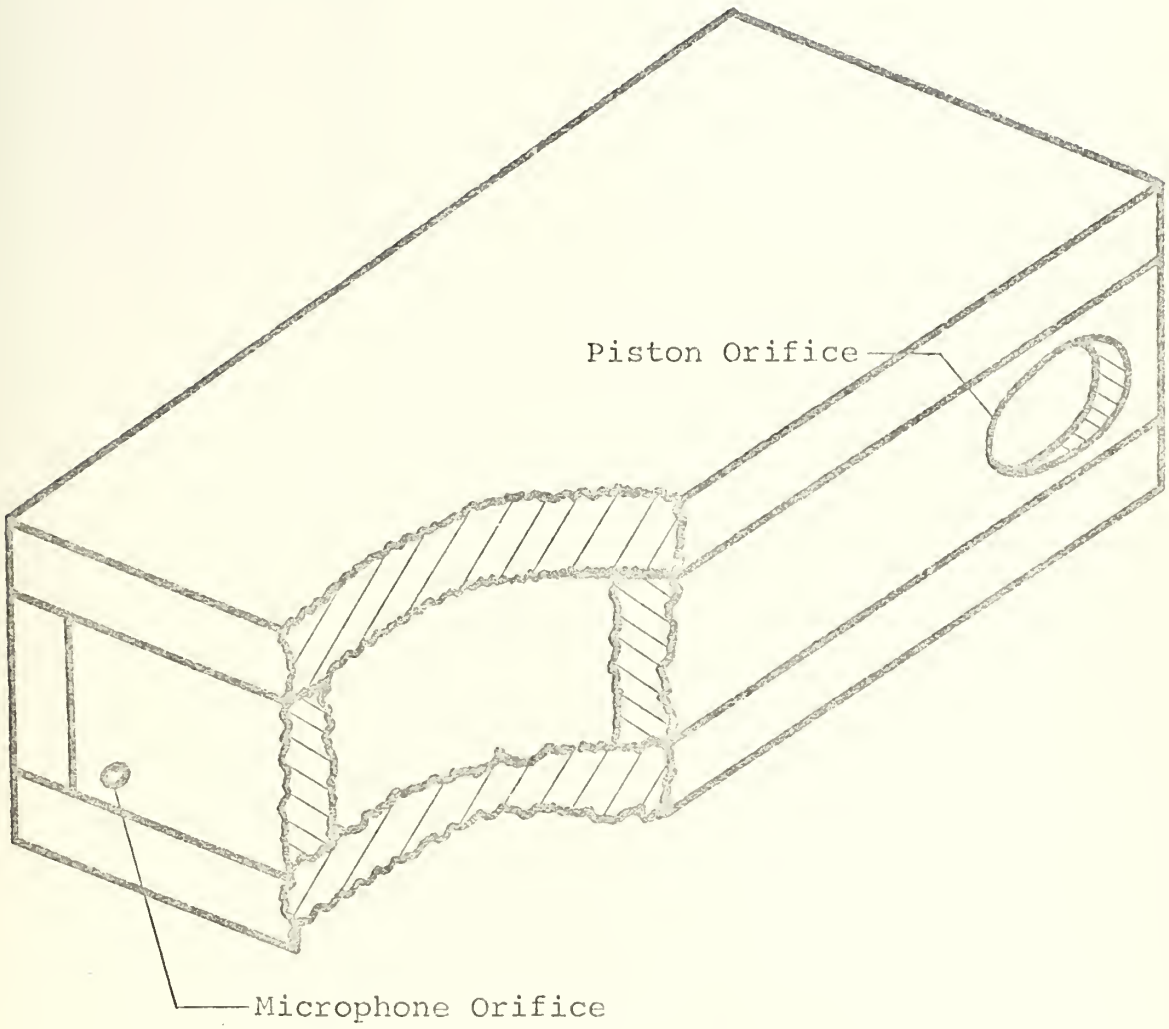

FIGURE 1. Rigid Walled Cavity

TABLE I

Mode	Frequency
100	687 Hz
010	825 Hz
110	1071 Hz
210	1600 Hz

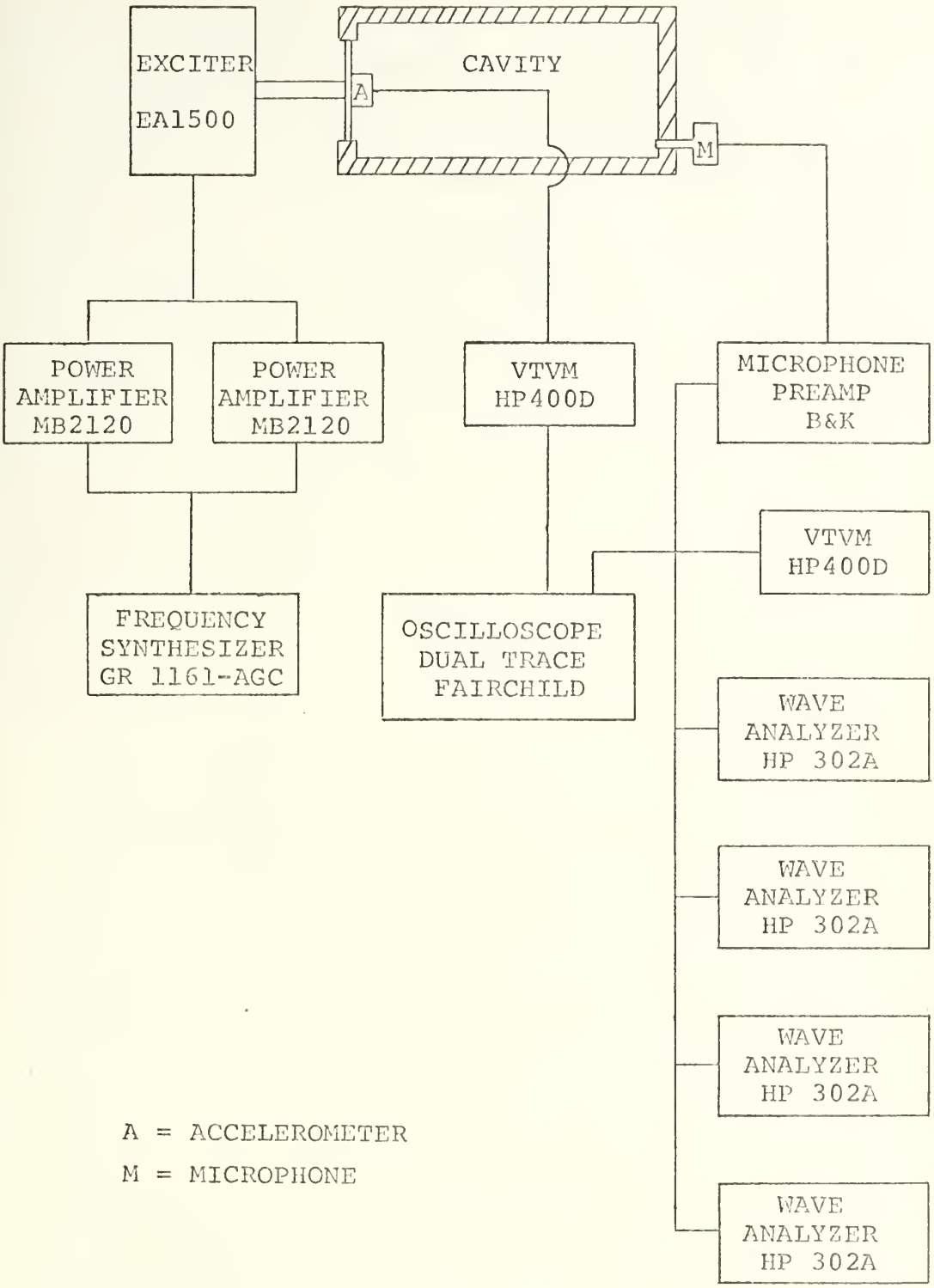

FIGURE 2. Apparatus

fundamental and harmonic components of the pressure wave were monitored by a 1/4 inch diameter Bruel and Kjar Type 4136 condenser microphone. It gained access to the cavity via the small orifice and its active element was flush with the interior of the cavity. It was fitted with an O-ring and sealed with high vacuum silicon grease. The output of the microphone system was monitored by a Hewlett Packard Model 400D vacuum tube voltmeter, the Fairchild Dual Trace Oscilloscope, and four Hewlett Packard Model 302A wave analyzers.

B. MICROPHONE OUTPUT AND STRENGTH PARAMETER

The investigation of the pressure waveform in the cavity required the calculation of the strength parameter from the observable quantities. The strength parameter is defined as

$$SP = MbQ_1,$$

$$M = \frac{P_1}{\rho C^2}$$

The microphone sensitivity was determined by piston phone calibration

$$S_m = (1.46 \pm 0.03)10^{-3} \text{ volt}/(\text{Nt}/\text{m}^2),$$

where

$$S_m = \frac{V}{P_{rms}},$$

and V is the rms voltage reading on the wave analyzer. The strength parameter can now be reformulated with observable or calculable quantities as

$$SP = \sqrt{2}\, VbQ_1/(S_m \rho c^2) \qquad (2)$$

C. FREQUENCY PARAMETER

The frequency parameter indicates the position of the driving frequency relative to the fundamental resonance frequency of the system. The frequency parameter is defined as

$$FP = 2(f_n - nf_1)\ Q_1/nf_1$$

D. CAVITY ISOLATION

To minimize the possible effects that could occur due to the vibration coupling of the cavity and exciter or cavity and table, the cavity and piston exciter was mechanically isolated with alternate slabs of wood and rubber. This restricted the interaction of the cavity with the piston to the piston orifice only.

VI. DATA TAKING PROCEDURES

A. PRERUN PROCEDURES

The modes of primary interest in this experiment were those that are in close proximity to one another, such as the 050 and 600 or the 330 and 420 modes. The relative position of a pair of modes could be adjusted by changing the position of the piston relative to the interior of the cavity. A quick frequency sweep at infinitesimal amplitudes revealed the relationships between the modes of interest. This procedure was repeated until the desired "tuned" condition was obtained.

> On two occasions significant changes in the frequencies of the modes occurred during a run. This was assumed to be caused by an unintentional movement of the piston with respect to the cavity. This was concluded as on both occasions the cavity had been repositioned on the morning of the run. To correct this problem, the cavity was run at infinitesimal amplitudes for an eight hour period and then allowed to sit overnight prior to a data session. After initiating this action, no further "settling-in" problems were encountered.

> As with Beech [12] and Lane [2] significant drifts in resonant frequency were noted during each session. This is most likely due to temperature variations. Prior to each data run, the cavity was activated at infinitesimal amplitudes for at least four hours. This prewarmed the cavity and was found to significantly reduce the rate of change of the fundamental frequency. However, this did not preclude the necessity of

taking numerous measurements of the fundamental during each run to establish a calibration curve. It was assumed that all harmonics drifted proportionally with the fundamental.

B. INFINITESIMAL AMPLITUDE ANALYSIS

An initial graphical representation of the linear response of the cavity was desirable as a guide in later more detailed measurements. This was achieved by setting the drive level at about 0.01 volts as indicated on the accelerometer VTVM. A plot was then made of the relative amplitudes (as measured on the microphone VTVM) versus frequency. This plot gave a visual display of the Q_n and E_n of each mode (see Figure 3).

If this plot looked sufficiently interesting, detailed measurements of the Q_n and E_n for each mode were performed. The microphone output voltage for each mode was maximized by varying the frequency. The frequency was then shifted until the voltage measured on the wave analyzer (in AFC) was -3dB below the maximum value. The difference between the frequencies of the -3dB points allowed the calculation of Q. It was assumed that the center frequency between the -3dB points was a good estimate of the resonance frequency. In some cases where the resonant peak was not symmetric, measurements were taken at the -3dB, -2dB and -1dB points. A linear plot of center frequency versus dB-down was extrapolated to 0dB to ascertain the resonance frequency. In a similar fashion a linear plot of Q versus dB-down was constructed to give an estimate of Q. The equations used for this extrapolation were

taking numerous measurements of the fundamental during each run to establish a calibration curve. It was assumed that all harmonics drifted proportionally with the fundamental.

B. INFINITESIMAL AMPLITUDE ANALYSIS

An initial graphical representation of the linear response of the cavity was desirable as a guide in later more detailed measurements. This was achieved by setting the drive level at about 0.01 volts as indicated on the accelerometer VTVM. A plot was then made of the relative amplitudes (as measured on the microphone VTVM) versus frequency. This plot gave a visual display of the Q_n and E_n of each mode (see Figure 3).

If this plot looked sufficiently interesting, detailed measurements of the Q_n and E_n for each mode were performed. The microphone output voltage for each mode was maximized by varying the frequency. The frequency was then shifted until the voltage measured on the wave analyzer (in AFC) was -3dB below the maximum value. The difference between the frequencies of the -3dB points allowed the calculation of Q. It was assumed that the center frequency between the -3dB points was a good estimate of the resonance frequency. In some cases where the resonant peak was not symmetric, measurements were taken at the -3dB, -2dB and -1dB points. A linear plot of center frequency versus dB-down was extrapolated to 0dB to ascertain the resonance frequency. In a similar fashion a linear plot of Q versus dB-down was constructed to give an estimate of Q. The equations used for this extrapolation were

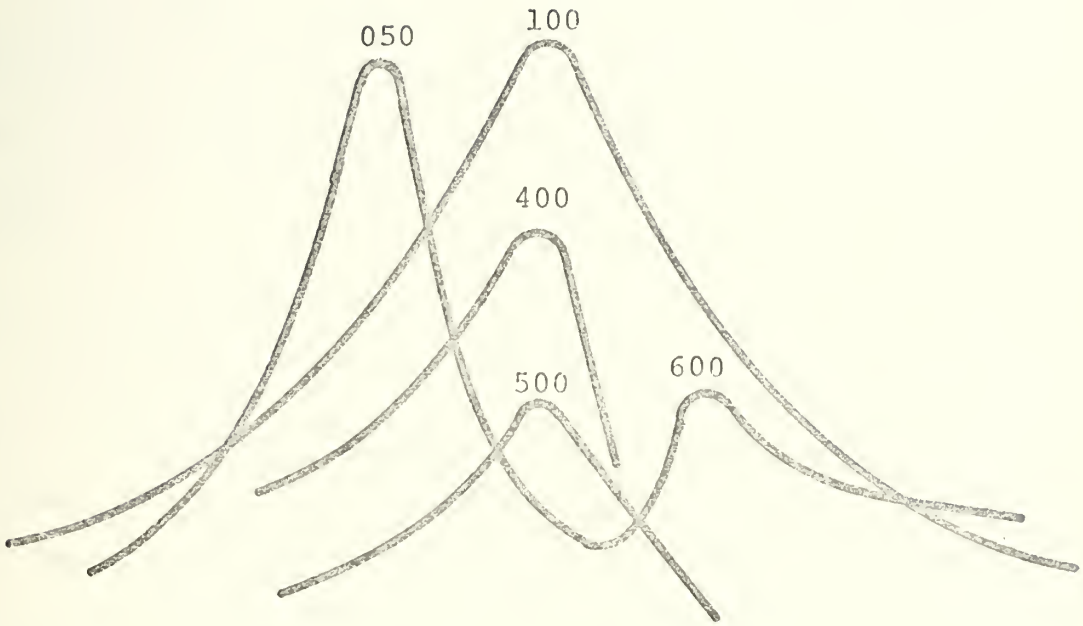

SCALE:

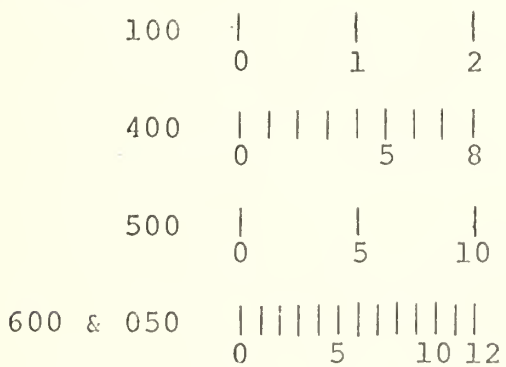

FIGURE 3. Linear Response Curves

$$3\text{dB} \qquad Q_n = \frac{\omega_{nr}}{\omega_{n+} - \omega_{n-}}$$

$$2\text{dB} \qquad Q_n = 0.757 \frac{\omega_{nr}}{\omega'_{n+} - \omega'_{n-}}$$

$$1\text{dB} \qquad Q_n = 0.510 \frac{\omega_{nr}}{\omega''_{n+} - \omega''_{n-}}$$

where

ω'_{n+} and ω'_{n-} and ω''_{n+} and ω''_{n-} are the frequencies corresponding to the 2dB and 1dB points above and below ω_{nr}. The E_n were calculated from the resonance frequencies of the modes.

C. FINITE-AMPLITUDE ANALYSIS

After selection of a family of modes to be investigated, the Q of the gravest member was measured. From this the peak pressure of the fundamental was calculated from Equation 2 for the desired strength parameter. The choice of strength parameter was dependent upon the extent of the frequency sweep desired. As the frequency was moved off resonance, it was necessary to increase the drive level to keep the level of the fundamental constant. There is a limit to how far above and below resonance the frequency could be changed. At high driving levels the accelerometer output would distort The onset of distrotion was abrupt and easily observed on the oscilloscope and was also accompanied by an easily detectable distortion of sound coming from the cavity. This distortion always occurred at drive levels below the maximum permitted by the power amplifier. The higher the strength parameter, the narrower would be the distortion limited band inspected.

A bank of four wave analyzers was used allowing measurement of the 1st, 2nd, 3rd and 4th or 1st, 5th, 6th and 7th harmonics simultaneously. This promoted consistency between amplitude measurements. The peak pressure was maintained constant and the harmonic content was recorded for a range of frequency about the resonance frequency of the gravest member.

V. RESULTS

Figures 4 and 5 are the graphical representations of the cavity's linear response when excited at infinitesimal amplitudes in the vicinity of the theoretically degenerate modes 600 and 050. Cavity configurations A, B, and C correspond to different piston positions within the orifice. Configuration A has the piston flush with the interior cavity and B has the piston withdrawn into the orifice, and in C the piston is withdrawn even further into the orifice. In Figure 4 each Configuration has been aligned with six times the resonance frequency of the 100 mode. Figure 5 has been aligned with five times the resonance frequency of the 010 mode. Observe that both amplitude and relative position of each peak changes substantually with different piston positions. Significantly no clear distinction can be made by simple observation as to which family of modes each peak belongs.

Figures 6 and 7 represent cavity response in the vacinity of three times the resonance frequency of the 110 mode or two times the resonance frequency of the 210 mode. Each configuration has been aligned as explained in Figures 4 and 5. In Configuration D, the piston is nearly flush with the interior of the cavity and Configuration G corresponds to the furthest displacement of the piston within the orifice. Observe that with Configuration F, both peaks have merged and in Configuration G a third peak has appeared. This peak is thought to be the 040 mode, but has not been positively identified.

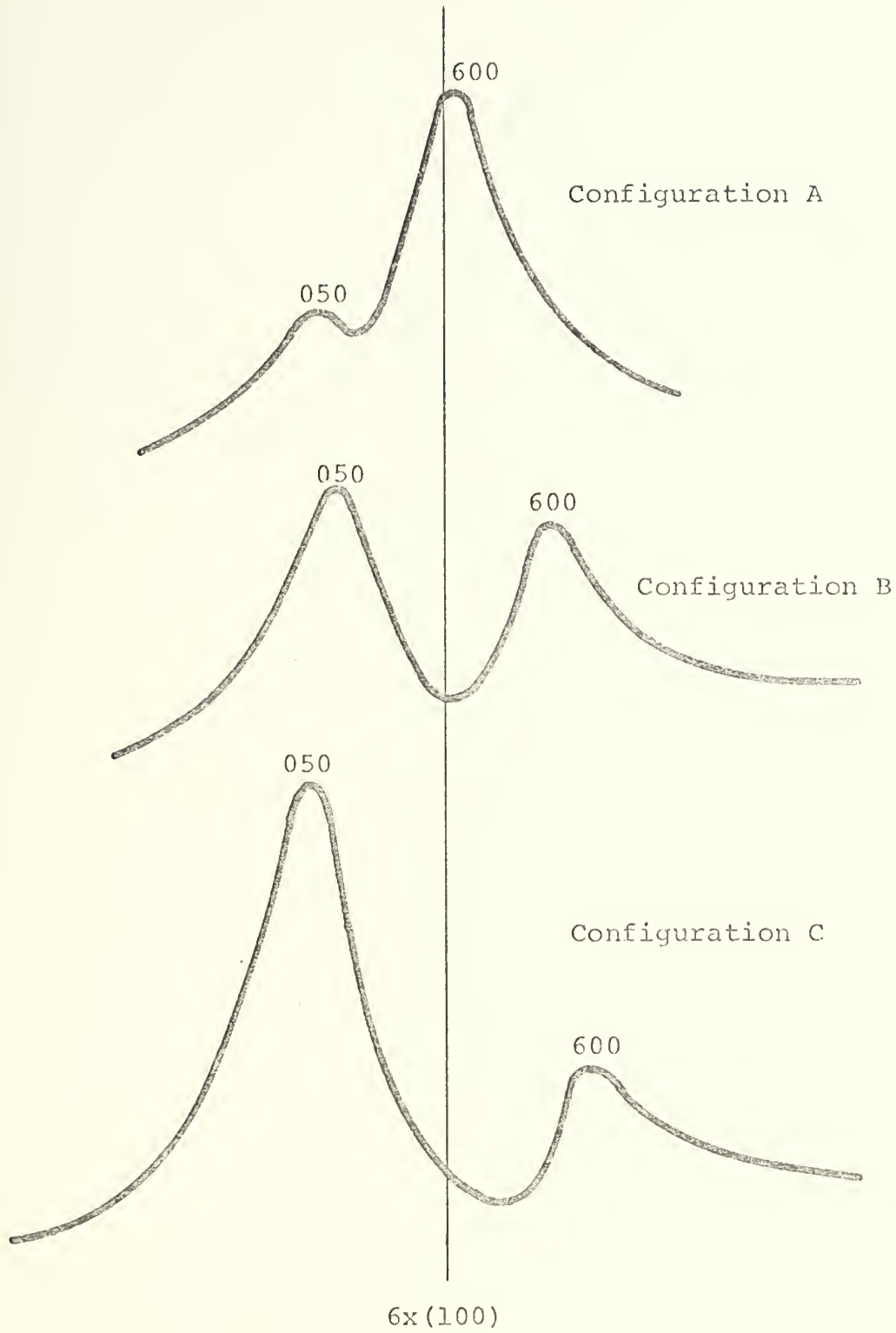
600
Configuration A
050
050
600
Configuration B
050
Configuration C
600
6x(100)

FIGURE 4

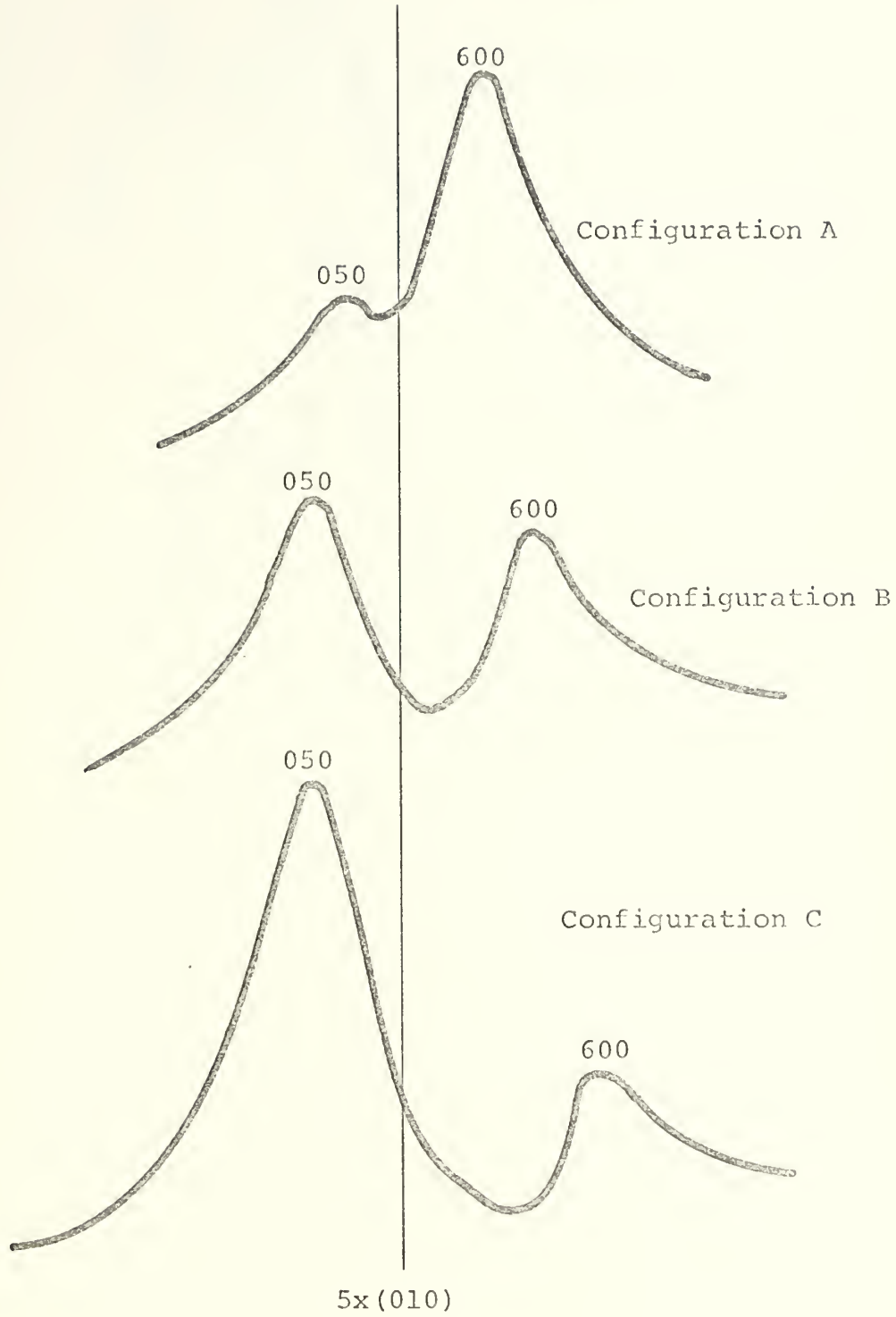
600
Configuration A
050
050
600
Configuration B
050
Configuration C
600
5x(010)

FIGURE 5

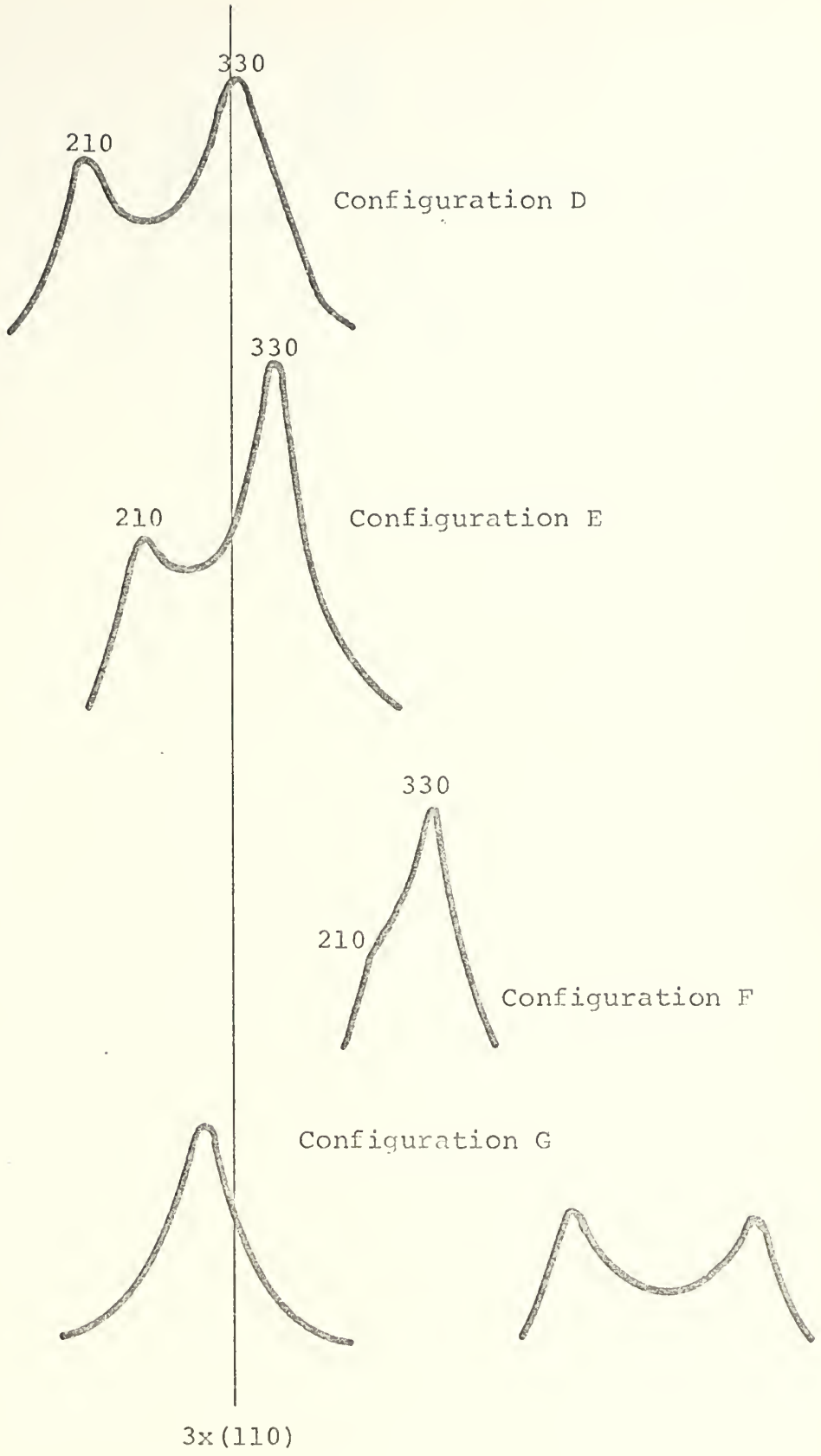
330
210
Configuration D
330
210
Configuration E
330
210
Configuration F
Configuration G
3x(110)

FIGURE 6

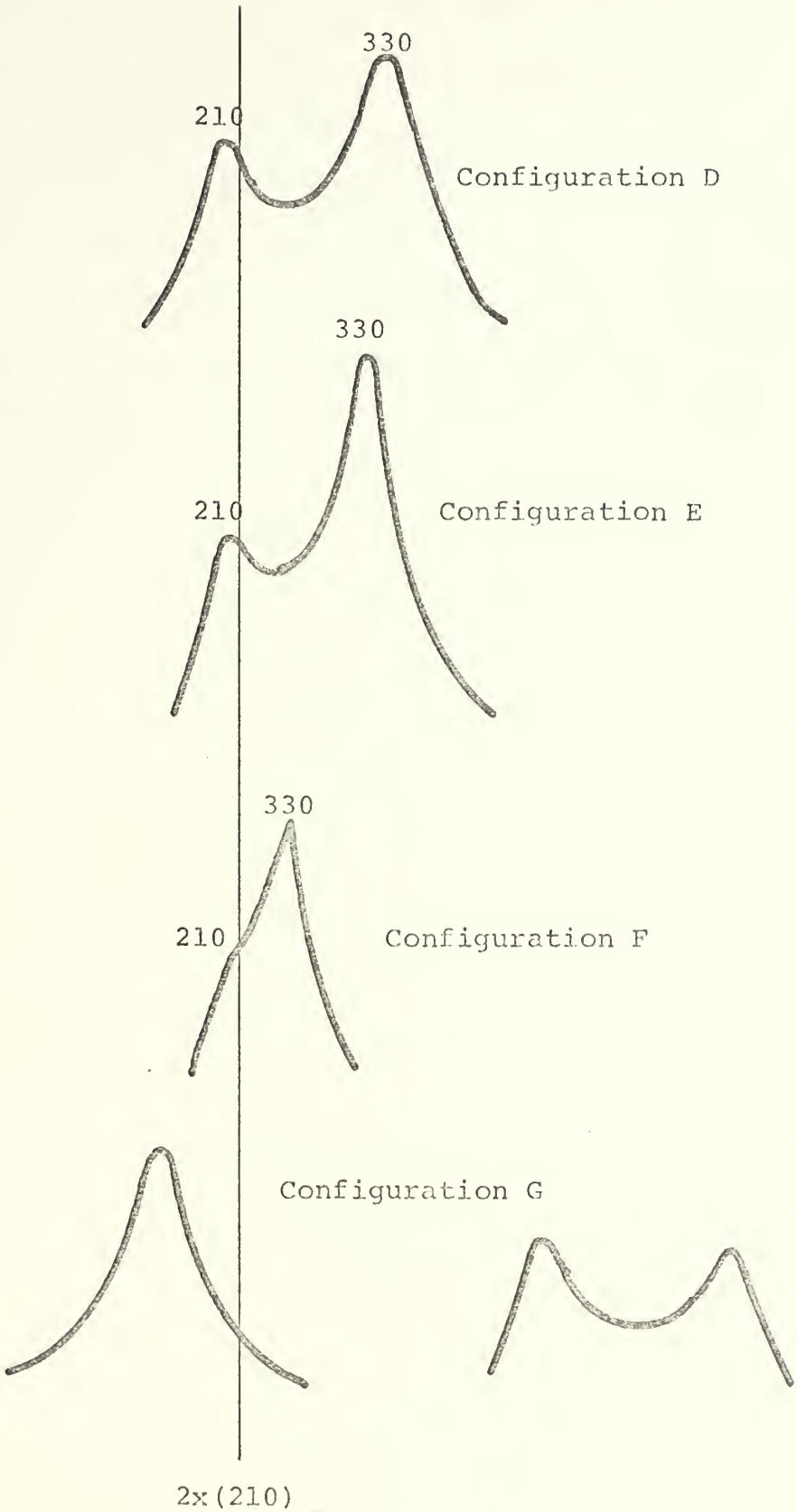
330
210
Configuration D
330
210
Configuration E
330
210
Configuration F
Configuration G
2x(210)

FIGURE 7

Tables II through XV present the data for the linear, infinitesimal-amplitude region. The information on the empirical losses is contained in the Q_n and E_n. Each table corresponds to a particular family of modes. When an extrapolation to 0dB has been made, 3dB, 2dB and 1dB data has been included. For Configurations E and F mode overlap was so complete that it was necessary to estimate Q from average values of Q for the same mode for other adjacent configurations. Estimation of E was carried out by inspection of Figures 6 and 7.

The values from the tables were used in the computer program to predict the harmonic distortion curves in Figures 9 and 11 through 23. The theoretical curves in these figures are plotted along with experimentally measured values of harmonic content. The theoretical predicted results are indicated as solid curves and measured values were plotted as solid symbols. Data were taken and theoretical predictions were made for strength parameters of 0.50 for driving the 100 mode, 010 mode and the 110 mode. A strength parameter of 0.25 was used for the 210 mode.

An initial problem was to ascertain which peak belonged to a particular family when two or more peaks occurred in close proximity as seen in Figures 4, 5, 6, and 7. This was solved by using the Q's and E's of each peak to generate a theoretical prediction. The theoretical prediction was then compared to the experimentally measured values. If good agreement between predicted and measured values was found, then the peak was considered identified. Figures 8, 9, 10, and 11 illustrate this technique with Configuration C.

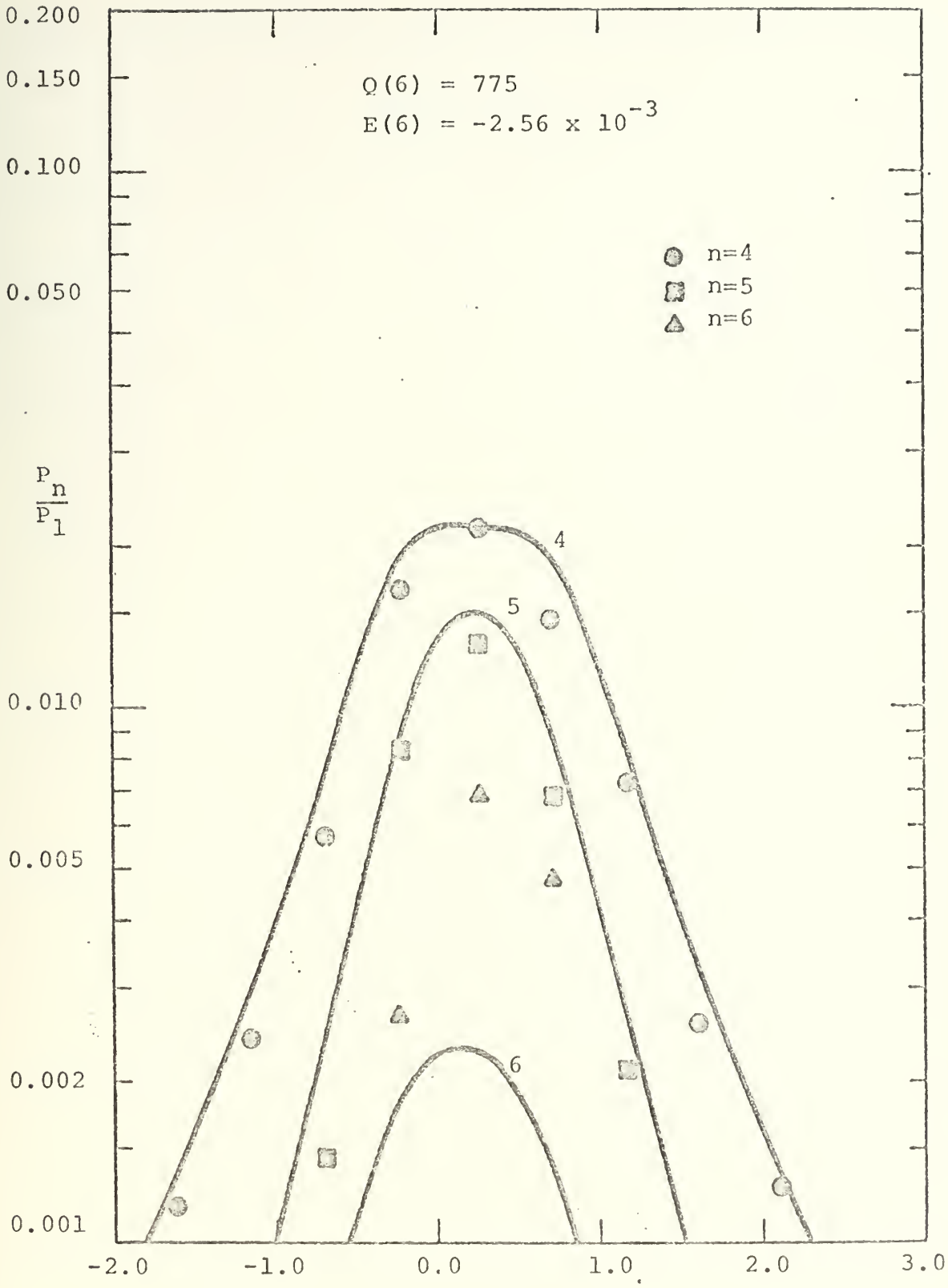

Configuration C 100 Mode SP=0.500

FIGURE 8

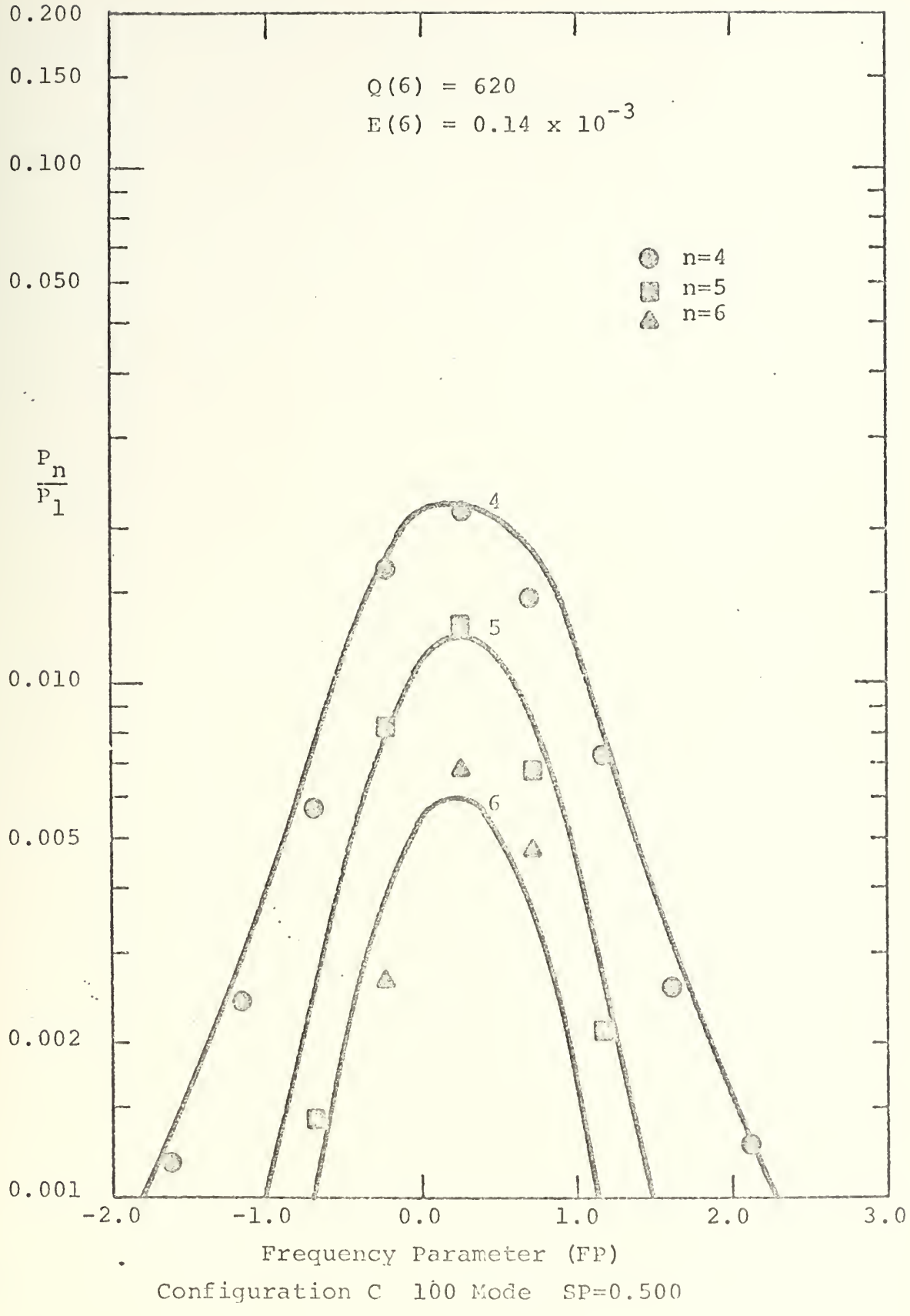
0.200
0.150
0.100
0.050
0.010
0.005
0.002
0.001
Q(6) = 620
E(6) = 0.14 x 10^-3
n=4
n=5
n=6
P_n / P_1
4
5
6
-2.0
-1.0
0.0
1.0
2.0
3.0
Frequency Parameter (FP)
Configuration C 100 Mode SP=0.500

FIGURE 9

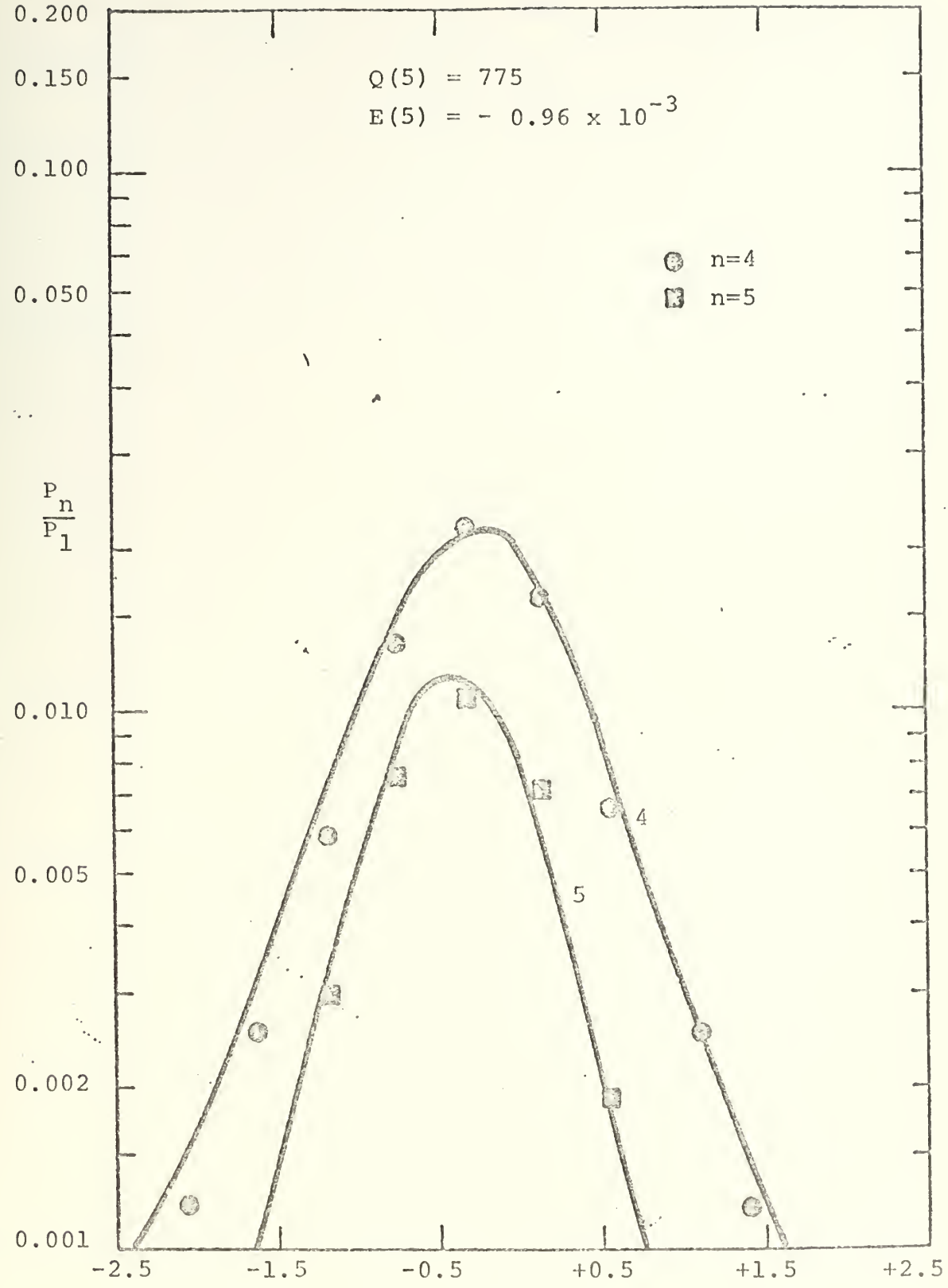

Configuration C 010 Mode SP=0.500

FIGURE 10

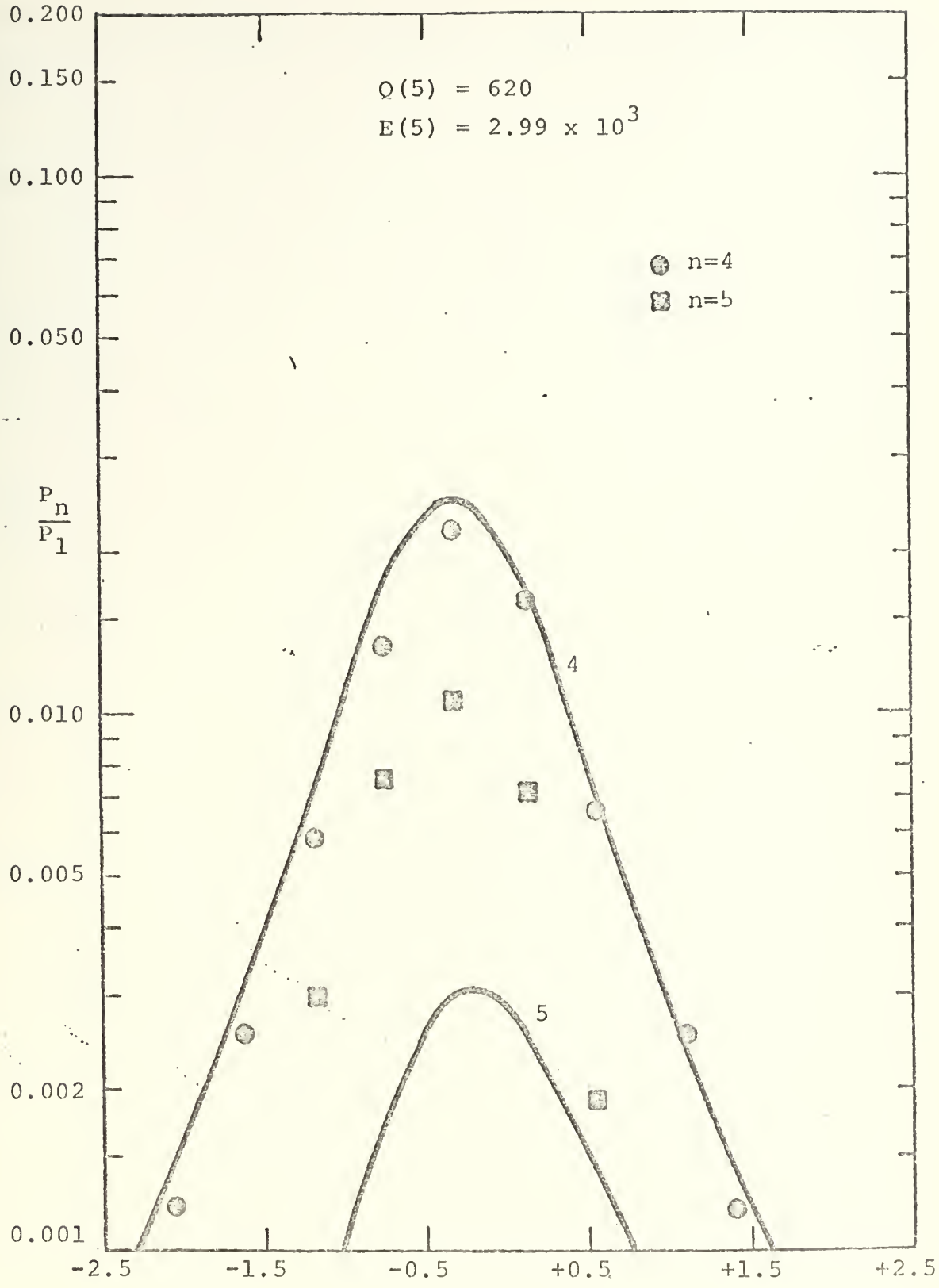

Configuration C 010 Mode SP=0.500

FIGURE 11

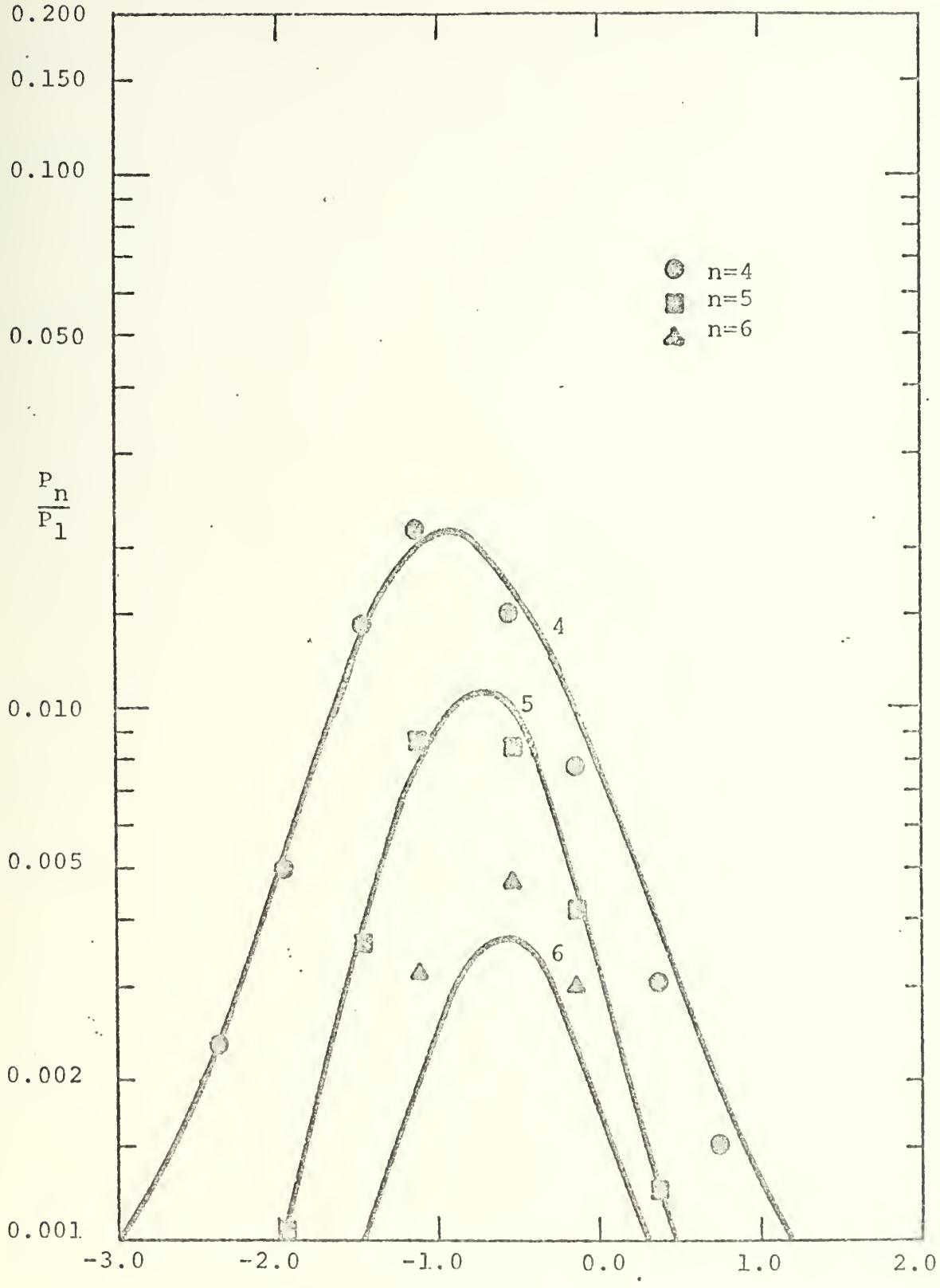

Configuration A 100 Mode SP=0.500

FIGURE 12

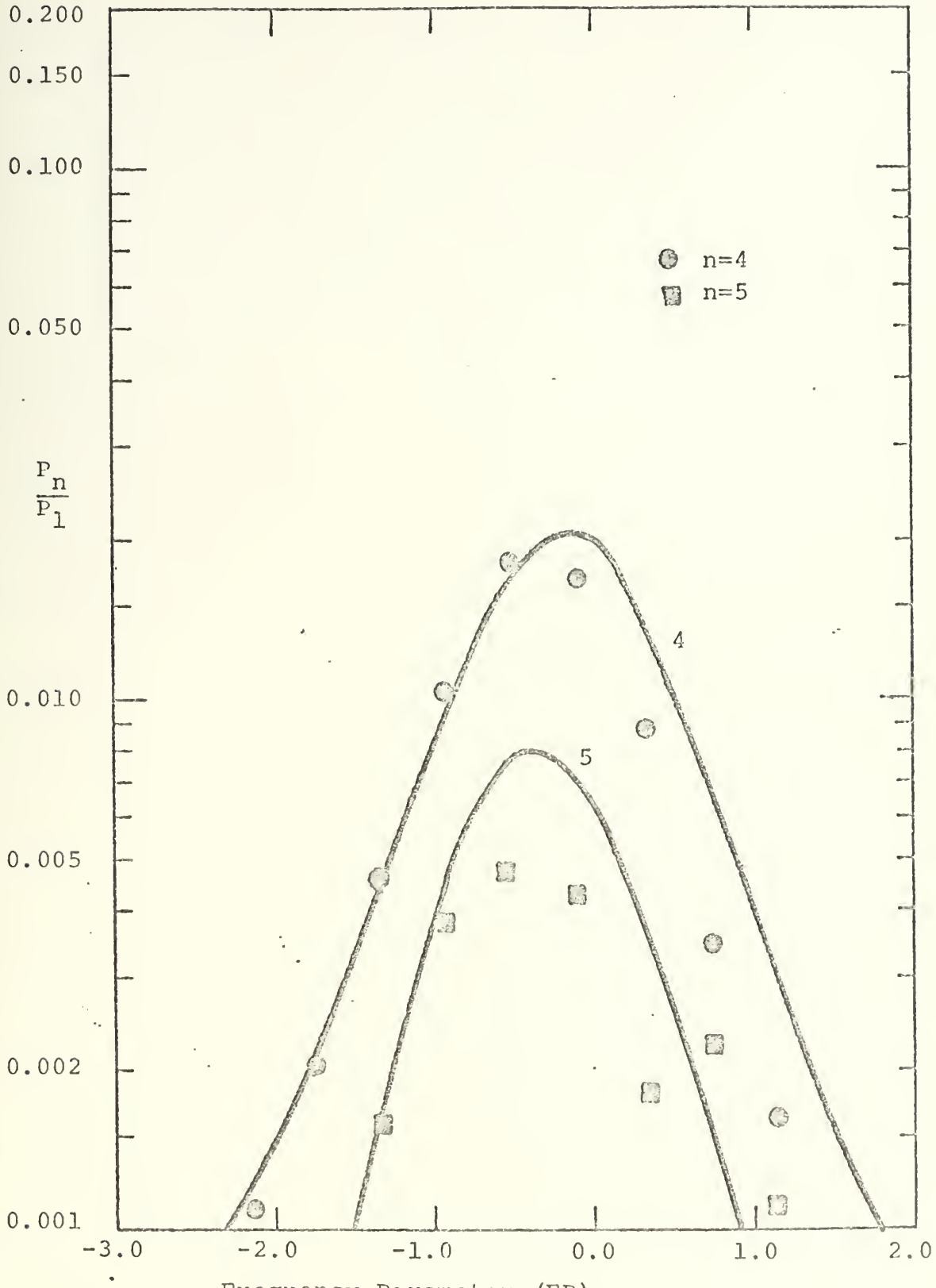

Configuration A 010 Mode SP=0.500

FIGURE 13

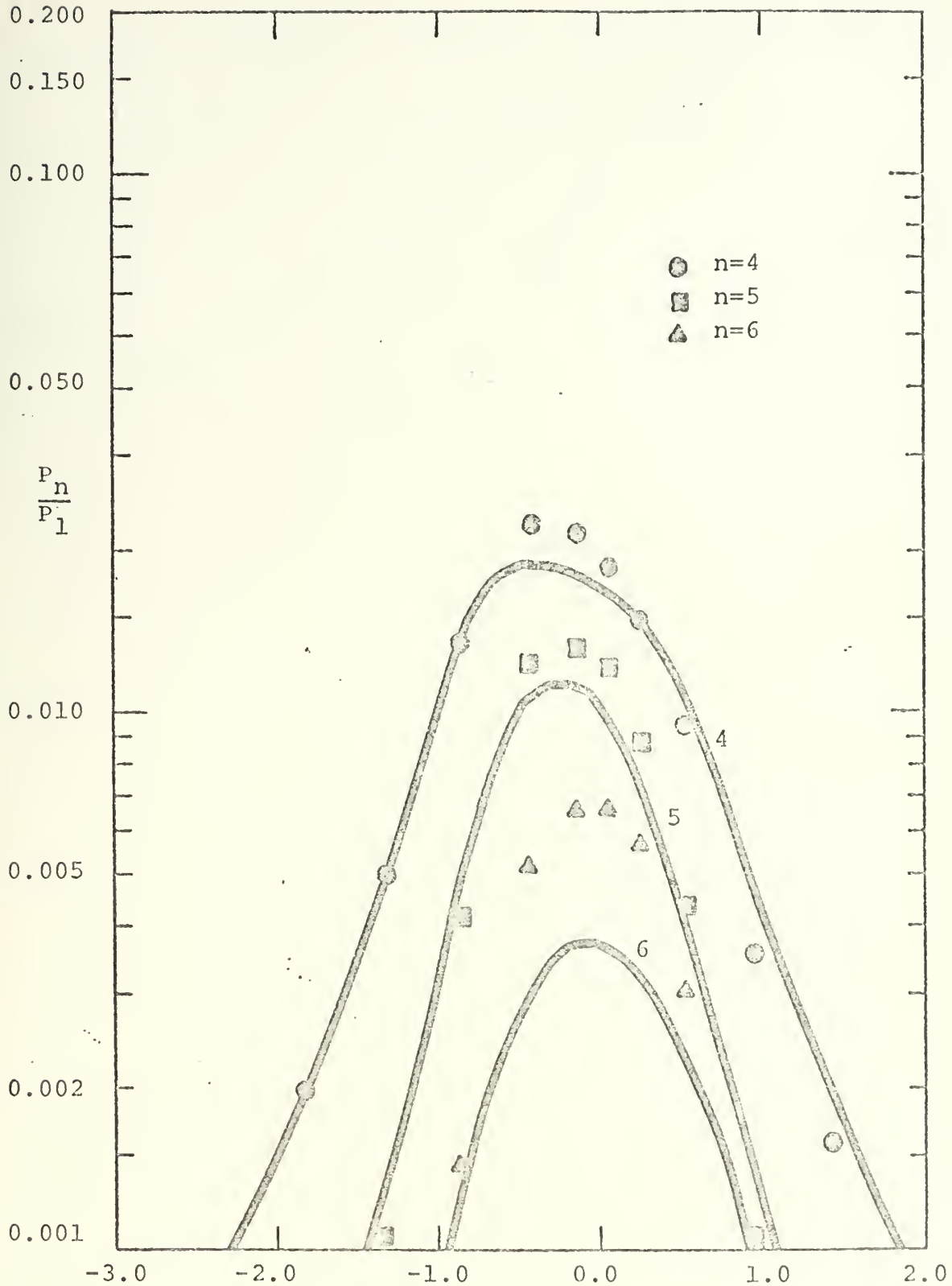

Configuration B 100 Mode SP=0.50

FIGURE 14

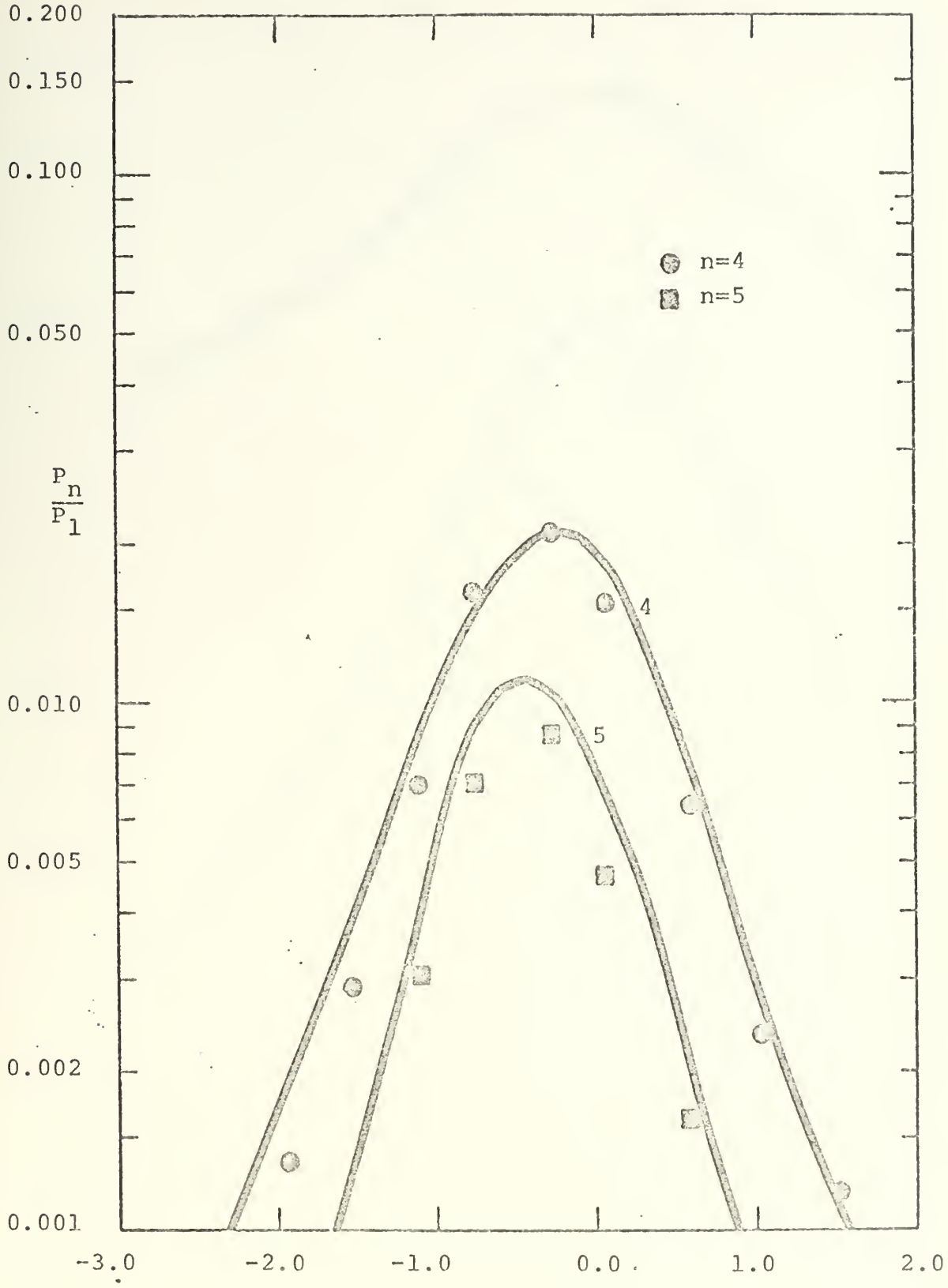

Configuration B 010 Mode SP=0.500

FIGURE 15

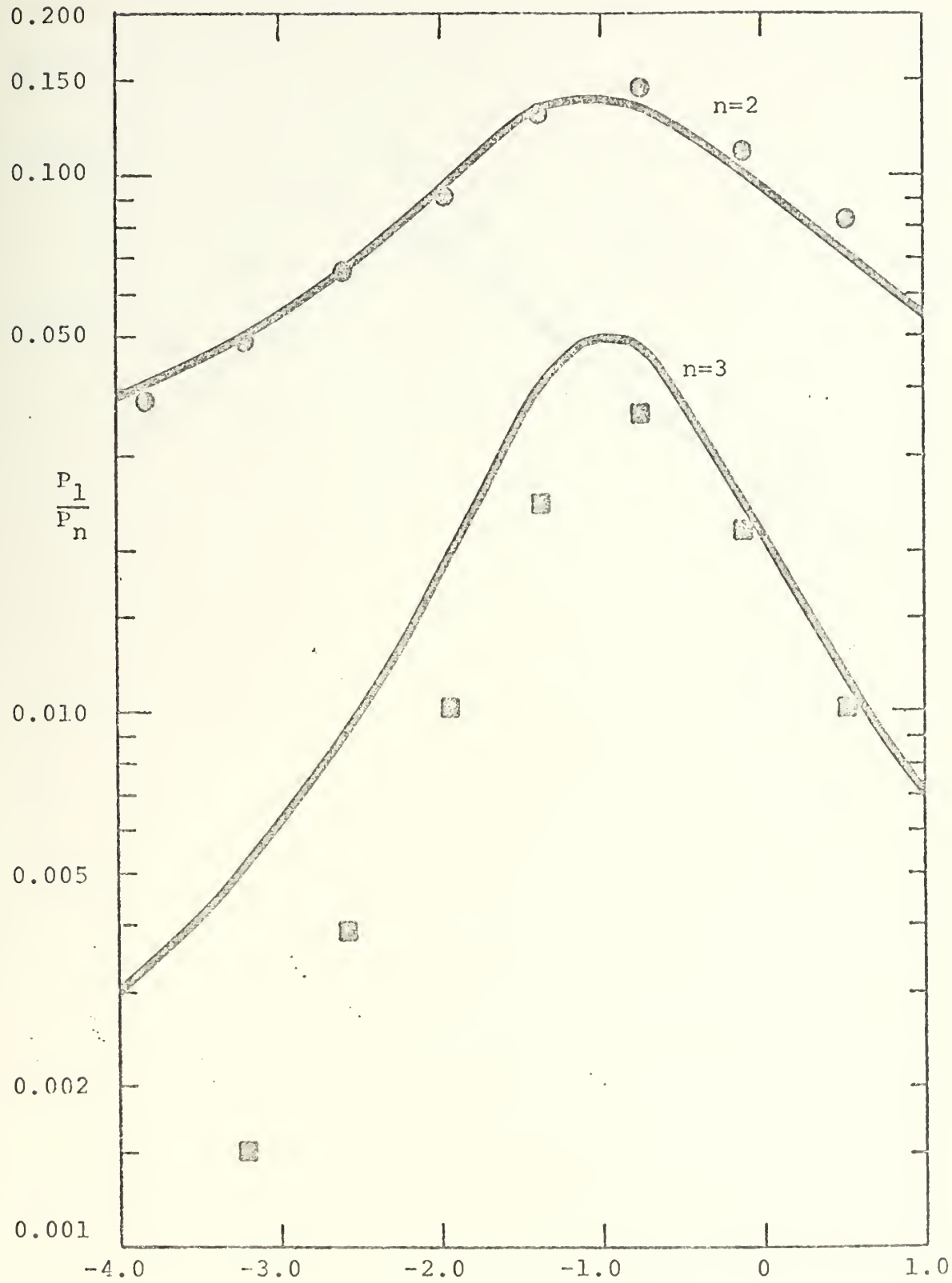

Configuration D 110 Mode SP=0.500

FIGURE 16

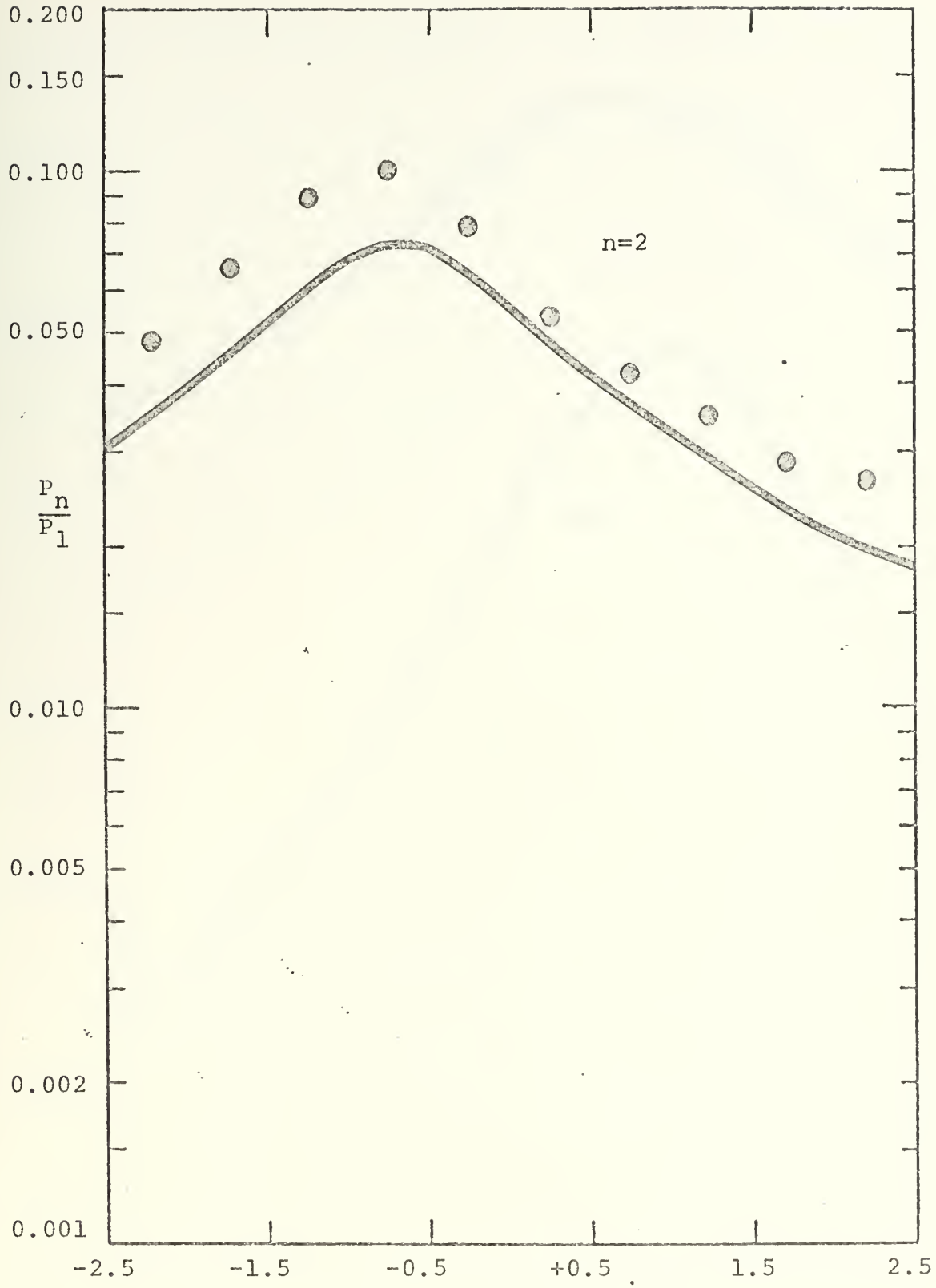

Configuration D 210 Mode SP=0.250

FIGURE 17

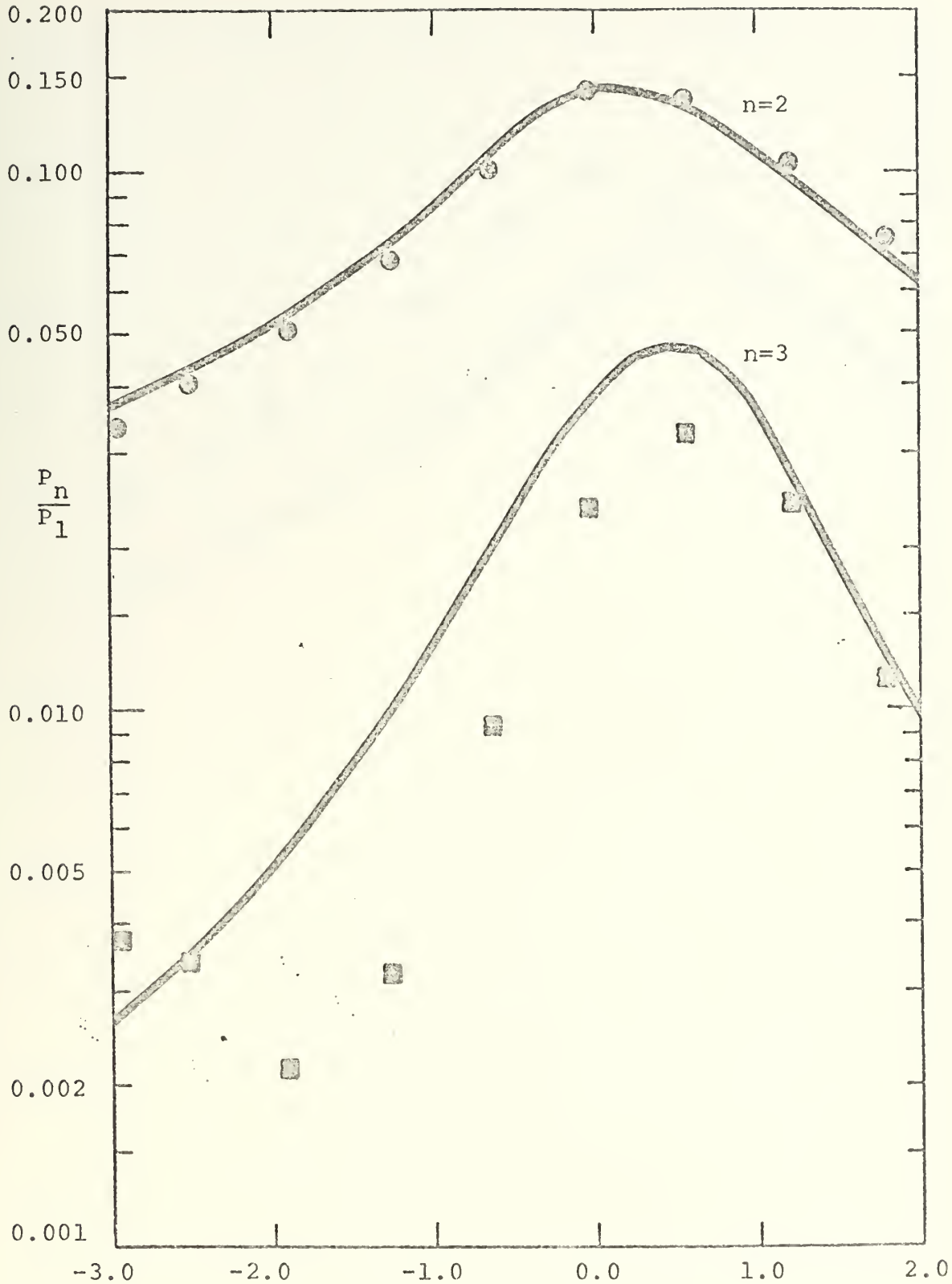

Configuration E 110 Mode SP=0.500

FIGURE 18

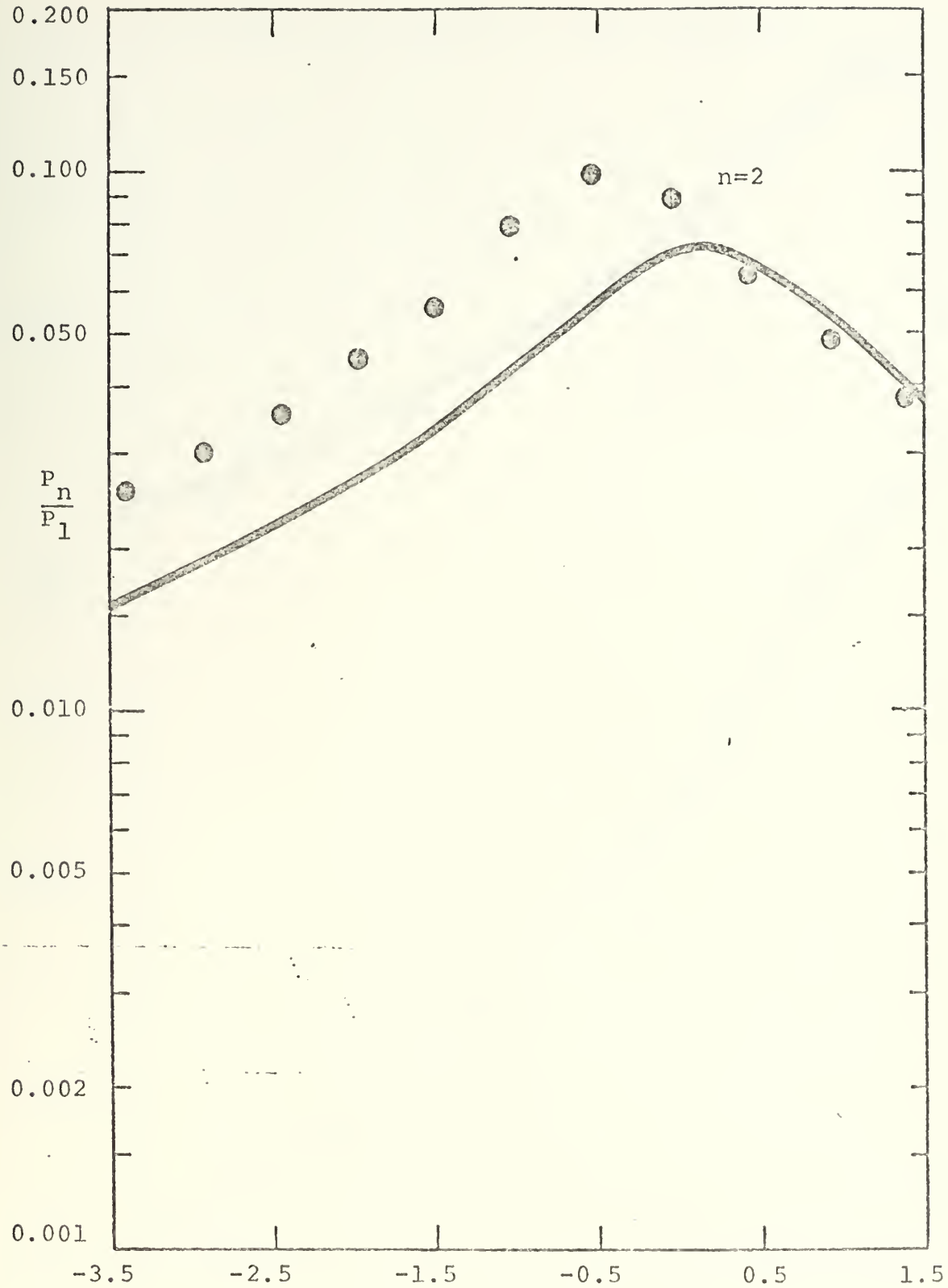

Configuration E 210 Mode SP=0.250

FIGURE 19

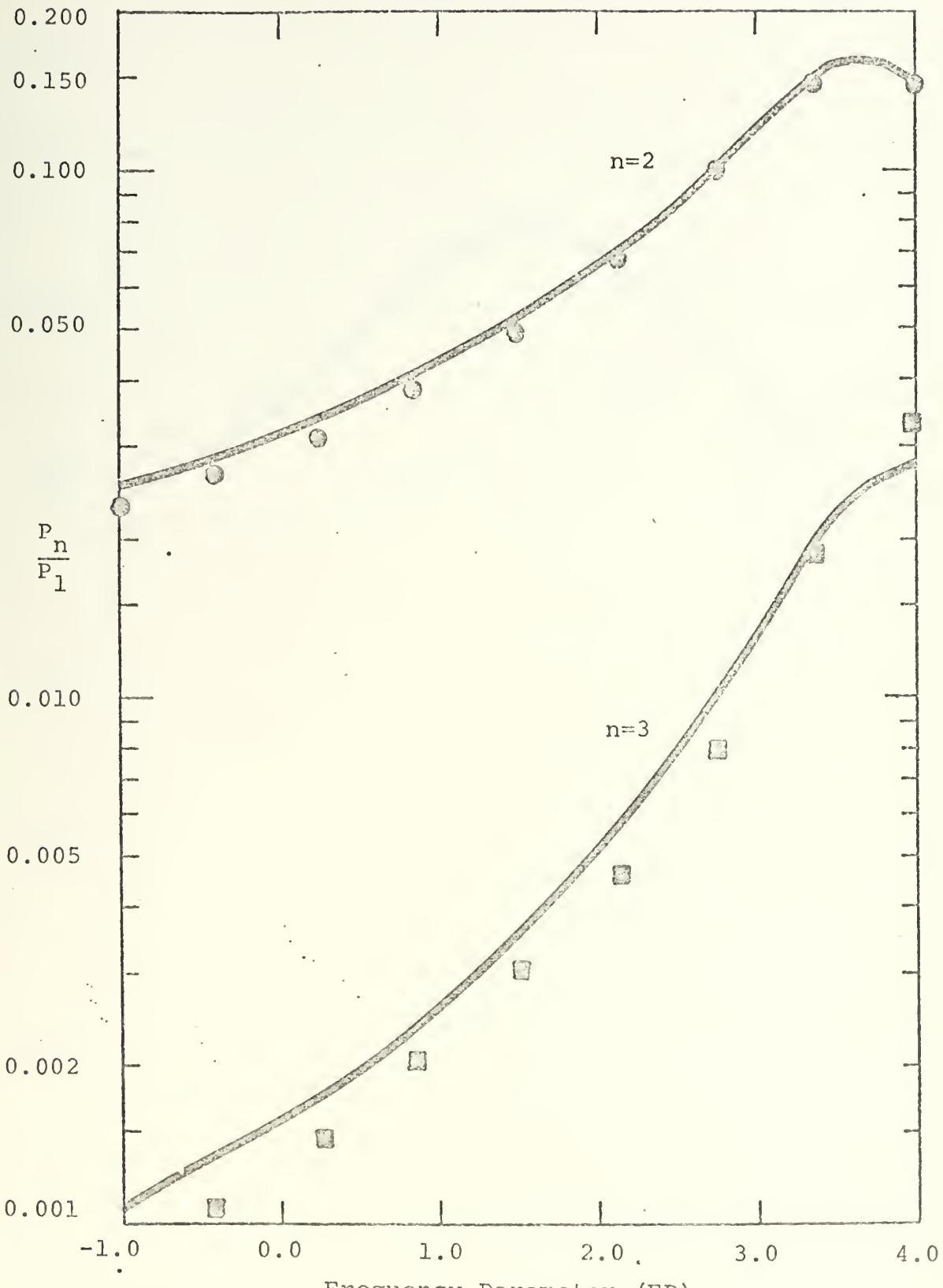

Configuration F 110 Mode SP=0.500

FIGURE 20

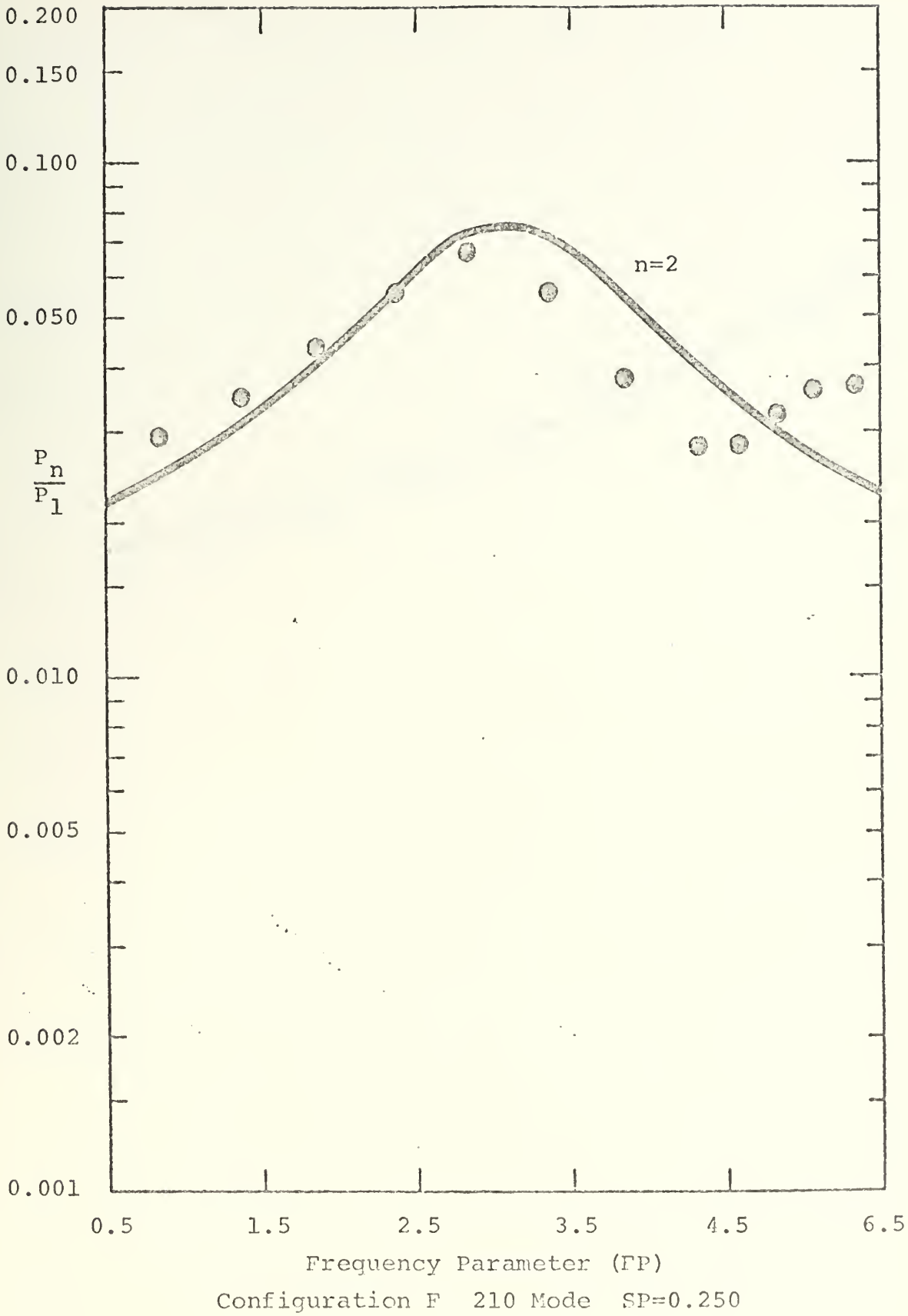

Configuration F 210 Mode SP=0.250

FIGURE 21

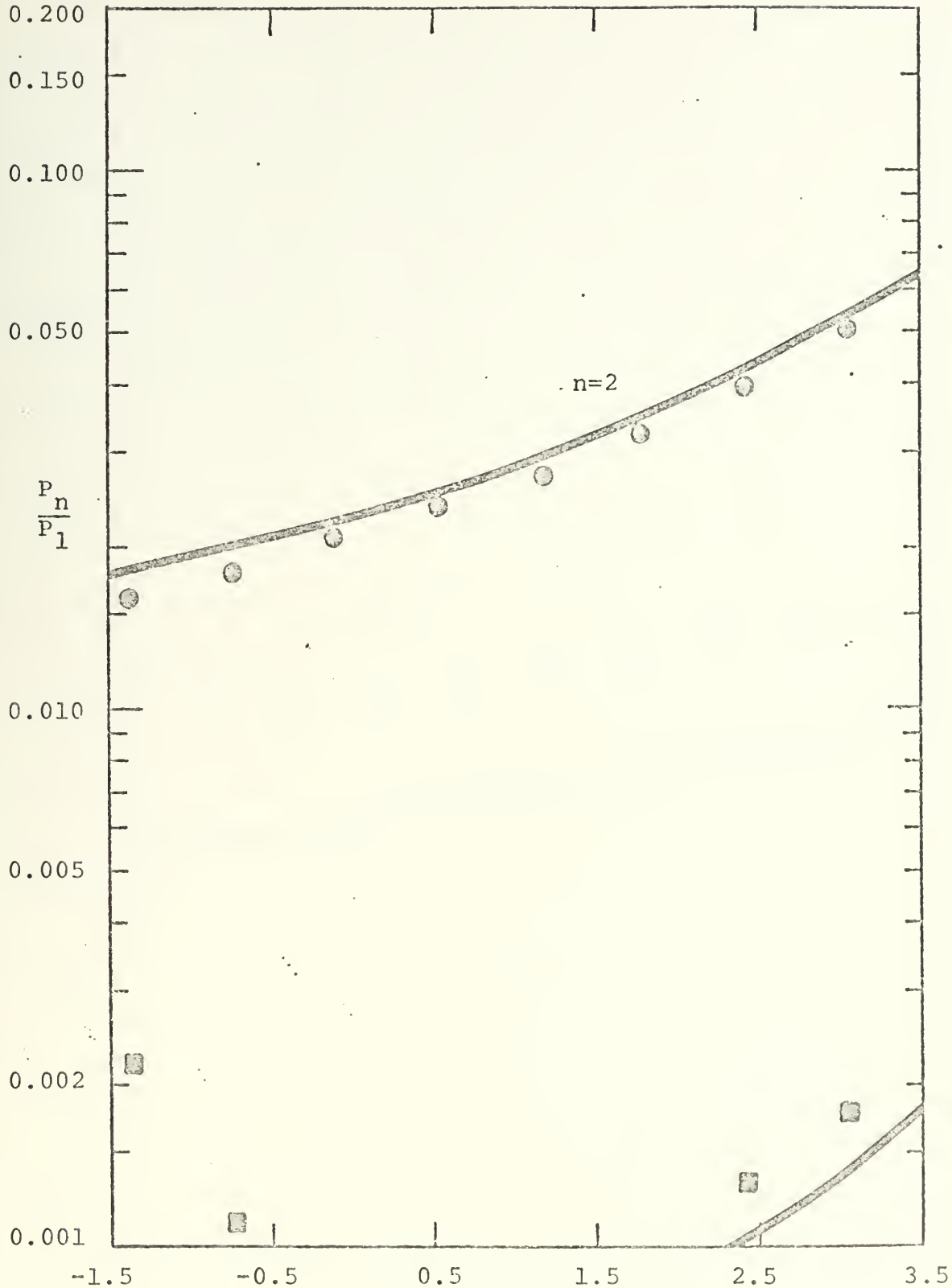

Configuration G 110 Mode SP=0.500

FIGURE 22

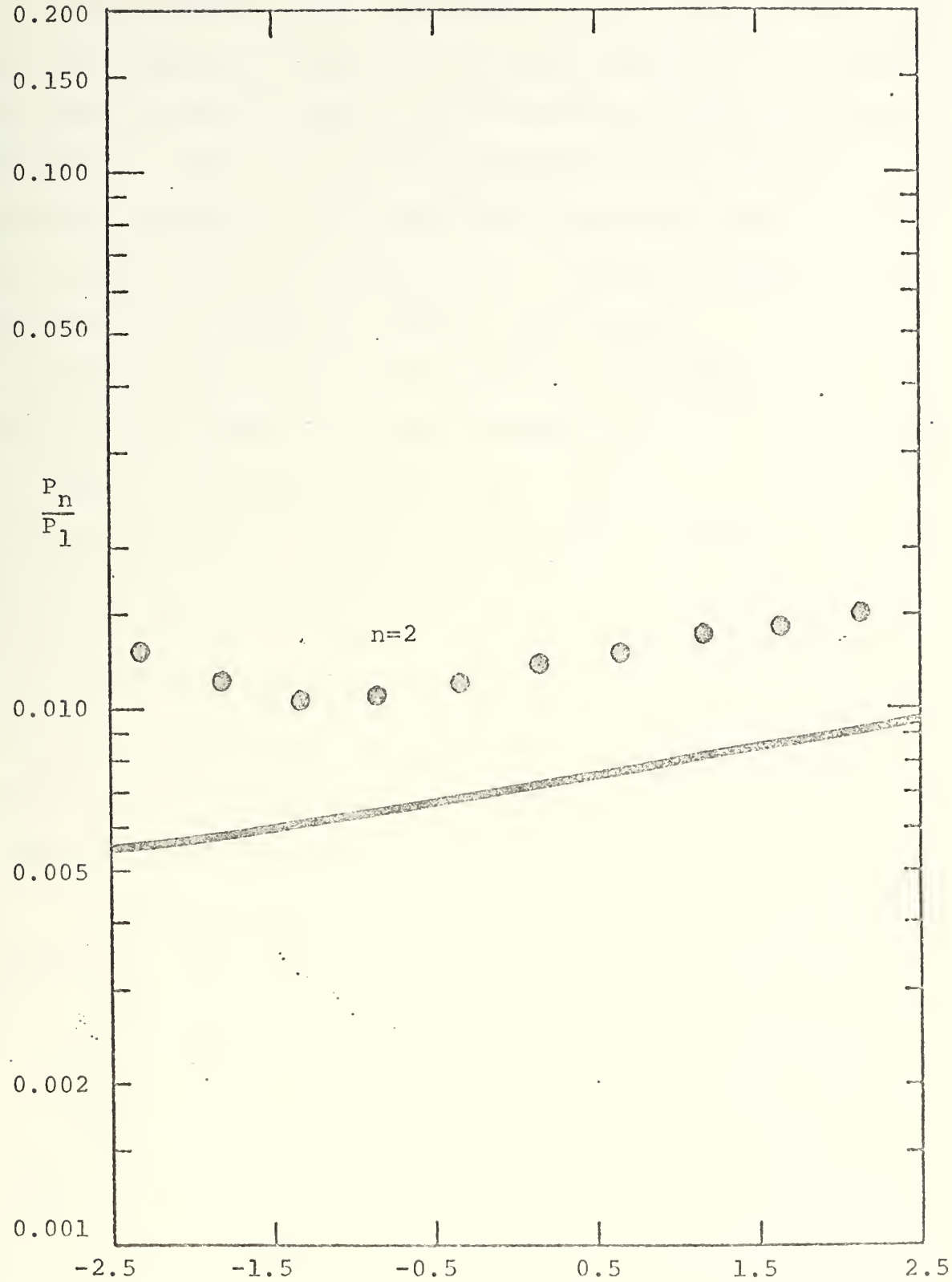

Configuration G 110 Mode SP=0.250

FIGURE 23

The experimental data in Figures 8 and 9 are identical and were obtained by driving the cavity at frequencies near the resonance of the 100 mode. The theoretical results are calculated from the same Q_n and E_n except for Q(6) and E(6). Figure 8 contains the Q(6) and E(6) calculated from the left peak of Configuration C on Figure 4. Figure 9 contains the Q(6) and E(6) calculated from the right peak.

The good agreement between measured and predicted values exhibited by Figure 9 is clear evidence that the right-hand peak in Figure 4 represents the 600 mode. Additional verification is shown in Figures 10 and 11 which contain experimental data measured by driving the 010 mode and the same Q_n and E_n except for Q(5) and E(5). Figure 10 contains the Q(5) and E(5) from left peak of Configuration C on Figure 4 and Figure 11 contains the Q(5) and E(5) from the right peak. The good agreement shown in Figure 10 identifies the left peak in Figure 4 as belonging to the 050 mode.

In a similar manner, all peaks with the exception of Configuration G were identified and recorded on Figures 4, 5, 6, and 7. The E_n in the case of Configuration G were so large that positive identification was not possible.

Figures 9, 10, 12, 13, 14, and 15 are comparisons of measured data and theoretical predictions of the 100 modes and 010 modes for Configurations A, B, and C. Figures 15 through 21 are comparisons of the 110 modes and the 210 modes for Configurations D, E, F, and G. Figures 9, 10, 12, 14, 15, 17, and 20 exhibit good agreement between predicted and measured values. Figures 13, 16, 18, 21, 22, and 23 exhibit significant differences

between measured data and theoretical predictions in the vacinity of the peak of the non-family member. This indicates that some coupling has occurred within the cavity which has populated the non-family member. Figure 19 is considered to be in agreement with theory, but differs due to the estimated value of E. Figure 23 indicates a coupling with the 210 modes and 010 modes.

TABLE II

n00 Mode			Configuration A				
n		f_- (Hz)	f_+ (Hz)	f (Hz)	f_n (Hz)	Q	E x 10^3
1		686.05	688.23	2.18	687.14	315	0
2		1371.31	1374.42	3.11	1372.86	440	-1.20
3		2057.28	2061.43	4.15	2059.36	496	-1.25
4		Extrapolated to odB			2745.03	555	-1.69
	3dB	2741.91	2746.93	5.02	2744.42	537	
	2dB	2742.87	2746.71	3.84	2744.79	542	
	1dB	2743.80	2746.33	2.53	2745.06	552	
5		3432.34	3438.30	5.96	3435.32	578	-0.73
6		Extrapolated to 0dB			4130.23	690	+0.36
	3dB	4127.52	4133.79	6.27	4130.65	660	
	2dB	4128.26	4133.03	4.77	4130.65	660	
	1dB	4129.06	4132.17	3.11	4130.61	675	
1		687.25	689.40	2.15	688.32	319	0

TABLE III

0n0 Mode			Configuration A				
n		f_- (Hz)	f_+ (Hz)	f (Hz)	f_n (Hz)	Q	E x 10^3
1		823.38	825.66	2.28	824.52	360	0
2		1646.75	1650.08	3.33	1648.41	495	-0.44
3		2470.99	2475.34	4.45	2473.21	556	-0.37
4		3294.82	3300.50	5.68	3297.66	580	-0.46
5	1dB	4118.98	4122.86	3.88	4120.91	543	-1.03
1		824.04	826.32	2.28	825.18	360	0

TABLE IV

n00 Mode		Configuration B					
n		f_- (Hz)	f_+ (Hz)	f (Hz)	f_n (Hz)	Q	E x 10^3
1		686.04	688.16	2.12	687.10	323	0
2		1372.28	1375.26	2.98	1373.78	462	-0.40
3		2059.50	2063.41	3.91	2062.46	528	+0.39
4		Extrapolated to 0dB			2746.87	625	-0.79
	3dB	2743.86	2748.68	5.22	2746.46	528	
	2dB	2744.81	2748.43	3.62	2746.62	575	
	1dB	2745.74	2748.06	2.32	2746.90	604	
5		3433.82	3438.88	5.06	3436.35	678	-0.18
6		Extrapolated to 0dB			4128.80	610	
	3dB	4126.21	4133.70	7.49	4129.95	552	
	2dB	4126.85	4132.47	5.62	4129.66	557	
	1dB	4127.72	4131.35	3.63	4129.53	580	
1		686.60	688.73	2.13	687.66	323	0

TABLE V

0n0 Mode	Configuration B					
n	f_- (Hz)	f_+ (Hz)	f (Hz)	f_n (Hz)	Q	E x 10^3
1	823.11	825.36	2.25	824.24	366	0
2	1646.29	1649.54	3.25	1647.91	507	-0.36
3	2469.84	2474.29	4.45	2471.06	557	-0.74
4	3293.82	3298.68	4.86	3296.25	677	-0.31
5	4115.90	4121.34	5.44	4118.62	758	-0.70
1	823.36	825.61	2.27	824.48	364	0

TABLE VI

n00 Mode		Configuration C					
n		f_- (Hz)	f_+ (Hz)	f (Hz)	f_n (Hz)	Q	E x 10^3
1		685.09	687.18	2.09	686.14	328	0
2		1367.26	1370.12	2.86	1368.69	480	+0.29
3		2052.67	2056.49	3.92	2054.63	646	+0.99
4		Extrapolated to 0dB			2744.97	675	+0.04
	3dB	2742.16	2746.69	4.53	2744.42	606	
	2dB	2743.00	2746.43	3.43	2744.72	605	
	1dB	2743.93	2746.12	2.19	2745.03	638	
5		3430.27	3435.26	4.99	3432.77	689	+0.28
6		Extrapolated to 0dB			4124.70	620	+0.14
	3dB	4122.34	4130.67	8.33	4126.50	494	
	2dB	4123.04	4128.87	5.83	4125.95	536	
	1dB	4123.82	4127.37	3.55	4125.59	594	
1		685.65	687.74	2.09	686.70	329	0

TABLE VII

0n0 Mode	Configuration C					
n	f_- (Hz)	f_+ (Hz)	f (Hz)	f_n (Hz)	Q	E x 10^3
1	822.35	824.52	2.17	823.44	379	0
2	1640.51	1643.69	3.18	1642.10	517	-0.36
3	2461.07	2465.14	4.07	2463.10	606	-0.43
4	3290.02	3294.89	4.87	3292.46	655	-0.45
5	4111.00	4116.34	5.34	4113.67	772	-0.96
1	822.61	824.84	2.23	823.72	369	0

TABLE VIII

nn0 Mode	Configuration D					
n	f_- (Hz)	f_+ (Hz)	f (Hz)	f_n (Hz)	Q	E x 10^3
1	1071.31	1074.49	3.18	1072.90	388	0
2	2140.37	2145.26	4.89	2142.82	440	-1.44
3	3210.98	3217.07	6.10	3215.02	527	-1.26
1	1071.46	1074.63	3.17	1073.05	338	0

TABLE IX

2nn0 Mode		Configuration D					
n		f_- (Hz)	f_+ (Hz)	f (Hz)	f_n (Hz)	Q	E x 10^3
1		1596.98	1600.99	4.01	1598.99	399	0
2		Extrapolated to 0dB			3195.25	487	-0.91
	2dB	3193.44	3199.65	6.21	3196.54	388	
	1dB	3194.02	3197.72	3.70	3195.87	439	
1		1597.21	1601.22	4.01	1599.21	398	0

TABLE X

nn0 Mode — Configuration E

n	f_- (Hz)	f_+ (Hz)	f (Hz)	f_n (Hz)	Q	E x 10^3
1	1064.77	1067.91	3.14	1066.35	340	0
2	2131.13	2135.90	4.77	2133.52	447	+0.30
3	3199.56	3205.48	5.92	3202.53	543	+0.83
1	1065.20	1068.32	3.12	1066.76	340	0

TABLE XI

2nn0 Mode — Configuration E

n	f_- (Hz)	f_+ (Hz)	f (Hz)	f_n (Hz)	Q	E x 10^3
1	1593.28	1597.33	4.05	1595.31	394	0
2	Estimated				480	-0.47
1dB	3188.84	3193.61	4.77	3191.22	341	+0.02
1	1593.75	1597.82	4.07	1595.88	392	0

TABLE XII

nn0 Mode — Configuration F

n	f_- (Hz)	f_+ (Hz)	f (Hz)	f_n (Hz)	Q	E x 10^3
1	1051.10	1054.21	3.11	1052.65	339	0
2	2114.64	2119.20	4.56	2116.92	464	+5.45
3	Estimated				550	+7.65
1	1051.36	1054.41	3.05	1052.89	345	0

TABLE XIII

2nn0 Mode — Configuration F

n	f_- (Hz)	f_+ (Hz)	f (Hz)	f_n (Hz)	Q	E x 10^3
1	1578.75	1582.68	3.93	1580.71	404	0
2	Estimated				500	3.79
1	1579.15	1582.94	3.79	1581.04	418	0

TABLE XIV

nn0 Mode — Configuration G

n		f_- (Hz)	f_+ (Hz)	f (Hz)	f_n (Hz)	Q	E x 10^3
1		1049.41	1052.51	3.10	1050.96	340	0
2		2116.30	2120.83	4.43	2118.51	479	7.72
3		Extrapolated to 0dB			3213.56	550	18.85
	3dB	3208.86	3216.11	7.25	3212.49	444	
	2dB	3210.42	3215.69	5.27	3213.05	457	
	1dB	3211.75	3215.14	3.39	3213.45	483	
1		1049.97	1053.04	3.07	1051.50	342	0

TABLE XV

2nn0 Mode — Configuration G

n		f_- (Hz)	f_+ (Hz)	f (Hz)	f_n (Hz)	Q	E x 10^3
1		1576.35	1580.28	3.93	1578.31	402	0
2		Extrapolated to 0dB			3191.93	518	+11.00
	3dB	3189.40	3196.29	6.89	3192.85	464	
	2dB	3195.05	3190.00	5.05	3192.52	480	
	1dB	3190.69	3193.94	3.25	3192.32	500	
1		1577.21	1581.10	3.89	1579.15	405	0

VI. CONCLUSIONS

The theoretical model can be used to identify the modes of a non-ideal, rigid-walled cavity provided the E_n are sufficiently small (see Figures 8, 9, 10, and 11).

The theoretical model in its present form fails to account for the excitation of modes other than those belonging to the family of the driven mode. This excitation was observed to occur only in the case of nearly degenerate modes. It is believed to be caused by some linear coupling mechanism within the cavity.

APPENDIX A

FINITE-AMPLITUDE DATA

TABLE XVI

Configuration A — Mode 100

FP	$P_4/P_1 \times 10^3$	$P_5/P_1 \times 10^3$	$P_6/P_1 \times 10^3$
-2.41	2.26	0.52	-
-2.00	5.15	1.06	-
-1.50	14.90	3.71	0.93
-1.08	22.62	9.00	3.24
-0.58	15.45	8.75	4.78
-0.16	8.00	4.27	3.09
+0.34	3.08	1.24	0.87
+0.76	1.49	-	-
+1.21	0.77	-	-

TABLE XVII

Configuration A — Mode 010

FP	$P_4/P_1 \times 10^3$	$P_5/P_1 \times 10^3$
-2.62	0.65	-
-2.19	1.14	-
-1.78	2.06	-
-1.36	4.76	1.59
-0.94	10.90	3.88
-0.52	18.80	4.94
-0.10	17.68	4.42
+0.32	9.13	1.82
+0.74	3.65	2.29
+1.16	1.65	1.14
+1.58	0.88	-

TABLE XVIII

Configuration B Mode 100

FP	$P_4/P_1 x10^3$	$P_5/P_1 x10^3$	$P_6/P_1 x10^3$
-2.30	0.95	-	-
-1.83	2.00	0.53	-
-1.35	5.05	1.05	-
-0.89	13.69	4.21	1.42
-0.42	23.10	12.62	5.16
-0.14	22.50	13.15	6.84
+0.05	18.91	12.20	6.84
+0.23	15.25	8.95	5.79
+0.51	9.48	4.42	3.05
+0.95	3.58	1.05	0.53
+1.45	1.58	0.58	-

TABLE XIX

Configuration B Mode010

FP	$P_4/P_1 x10^3$	$P_5/P_1 x10^3$
-2.39	0.77	-
-1.97	1.37	-
-1.54	2.97	0.65
-1.11	7.14	3.09
-0.68	16.65	7.14
-0.26	21.40	8.93
+0.08	16.08	4.82
+0.60	6.55	1.61
+1.03	2.38	0.59
+1.54	1.19	0.65
+1.88	0.71	0.77

TABLE XX

Configuration C — Mode 100

FP	$P_4/P_1 \times 10^3$	$P_5/P_1 \times 10^3$	$P_6/P_1 \times 10^3$
-2.13	0.59	-	-
-1.66	1.13	-	-
-1.18	2.47	0.59	-
-0.71	5.92	1.45	-
-0.23	17.20	8.60	2.68
+0.24	22.49	13.42	6.99
+0.71	15.05	6.99	4.84
+1.19	6.45	2.15	0.97
+1.66	2.68	0.91	-
+2.14	1.29	-	-

TABLE XXI

Configuration C — Mode 010

FP	$P_4/P_1 \times 10^3$	$P_5/P_1 \times 10^3$
-2.58	0.78	-
-2.10	1.20	-
-1.66	2.53	0.60
-1.22	6.03	3.01
-0.77	13.85	7.84
-0.33	22.88	10.85
+0.11	16.88	7.24
+0.55	6.64	1.93
+1.01	2.53	0.90
+1.43	1.21	-
+1.88	0.60	-

TABLE XXII

Configuration D — Mode 110

FP	$P_2/P_1 \times 10^3$	$P_3/P_1 \times 10^3$
-3.84	40.00	1.08
-3.22	51.90	1.55
-2.60	69.60	4.01
-1.97	96.60	10.22
-1.35	138.10	25.70
-0.72	151.90	37.28
-0.10	118.90	22.09
+0.56	84.30	10.21
+1.15	63.60	5.94
+1.78	51.99	4.01
+2.40	42.81	2.76
+3.04	36.42	2.10
+3.66	32.60	1.60

TABLE XXIII

Configuration D — Mode 210

FP	$P_2/P_1 \times 10^3$
-3.21	32.40
-2.72	38.90
-2.22	49.90
-1.73	68.20
-1.24	92.10
-0.74	102.50
-0.25	80.50
+0.24	56.50
+0.74	43.41
+1.23	35.60
+1.73	29.80
+2.22	27.21
+2.72	25.29
+3.22	24.61

TABLE XXIV

Configuration E — Mode 110

FP	$P_2/P_1 \times 10^3$	$P_3/P_1 \times 10^3$
-4.16	35.19	1.10
-3.54	41.75	1.27
-2.92	52.51	1.43
-2.29	73.30	4.14
-1.66	102.20	11.01
-1.03	149.20	29.01
-0.40	152.00	37.30
+0.23	116.10	22.19
+0.86	82.99	10.50
+1.49	60.08	5.81
+2.12	50.03	3.87
+2.74	41.42	2.76
+3.38	35.62	1.93

TABLE XXV

Configuration E — Mode 210

FP	$P_2/P_1 \times 10^3$
-3.46	26.22
-2.97	30.07
-2.49	36.48
-2.00	46.10
-1.53	58.99
-1.03	82.01
-0.55	102.50
-0.06	91.01
+0.43	67.30
+0.91	50.00
+1.40	39.70
+1.89	33.22
+2.37	29.41
+2.85	26.82
+3.34	24.28
+3.82	17.30

TABLE XXVI

Configuration F — Mode 110

FP	$P_2/P_1 \times 10^3$	$P_3/P_1 \times 10^3$
-4.55	12.20	0.86
-4.24	12.75	0.81
-3.92	13.60	0.78
-3.60	14.42	0.75
-3.30	15.27	0.72
-2.98	15.81	0.67
-2.34	17.75	0.61
-1.71	22.40	0.61
-1.06	23.32	0.75
-0.43	27.20	1.28
+0.21	31.95	1.44
+0.85	40.00	2.06
+1.49	51.40	3.06
+2.12	70.00	4.66
+2.77	100.50	8.04
+3.40	155.20	19.15
+4.04	155.20	34.70

TABLE XXVII

Configuration F — Mode 210

FP	$P_2/P_1 \times 10^3$
-4.22	12.78
-3.72	13.35
-3.20	14.14
-2.71	15.12
-2.20	15.91
-1.70	17.10
-1.20	18.72
-0.70	19.71
-0.19	22.49
+0.26	25.95
+0.81	30.21
+1.34	36.63
+1.82	46.00
+2.32	59.20
+2.82	71.10
+3.33	58.60
+3.83	38.79
+4.34	28.94
+4.58	29.59
+4.83	33.50
+5.08	37.41
+5.35	38.10
+5.58	39.40

TABLE XXVIII

Configuration G — Mode 110

FP	$P_2/P_1 x10^3$	$P_3/P_1 x10^3$
-4.62	9.77	2.18
-3.98	10.89	2.32
-3.33	12.00	2.37
-2.68	13.39	2.40
-2.04	14.50	2.32
-1.40	16.49	2.22
-0.75	18.41	1.17
-0.11	21.20	0.75
+0.53	24.00	0.84
+1.18	27.97	0.84
+1.81	33.50	0.98
+2.46	40.50	1.31
+3.10	52.50	1.79
+3.75	73.20	2.57
+4.40	106.00	4.19
+5.05	131.30	5.31

TABLE XXIX

Configuration G — Mode 210

FP	$P_2/P_1 x10^3$
-5.05	9.09
-4.82	9.42
-4.32	9.61
-3.82	10.32
-3.33	11.95
-2.83	12.99
-2.34	13.32
-1.84	11.69
-1.34	10.90
-0.85	10.99
-0.35	11.57
+0.15	12.48
+0.65	13.31
+1.14	14.15
+1.64	14.72
+2.13	15.91
+2.63	17.20
+3.12	18.51
+3.62	20.10
+4.12	22.02
+4.62	24.62
+5.12	27.85
+5.63	32.42

BIBLIOGRAPHY

1. Coppens, A. B., and Sanders, J. V., "Finite-Amplitude Standing Waves in Rigid Walled Tubes," J. Acoust. Soc. Am., V. 43, P. 516-529, March 1968.

2. Lane, C., Finite-Amplitude Waves in a Rigid Walled Cavity, Thesis, Naval Postgraduate School, Monterey, California, 1972. L 2568

3. Kirchoff, G., Ann. Phys, Leipzig, V. 134, P. 177-193, 1868.

4. Lamb, H., Dynamical Theory of Sound, 2d ed., Chap VI, Edward Arnold and Co., London, England, 1925.

5. Fay, R. D., "Successful Method of Attack on Progressive Finite Waves," J. Acoust, Soc. Am., V. 28, P. 910-914, September, 1956.

6. Fay, R. D., "Plane Sound Waves of Finite-Amplitude," J. Acoust. Soc. Am., V. 3, P. 222-241, 1931.

7. Blackstock, D. T., "Propagation of Plane Sound Waves of Finite Amplitude in Nondissipative Fluids," J. Acoust. Soc. Am., V. 34, P. 9-30, January 1962.

8. Keck, W., and Beyer, R. T., "Frequency Spectrum of Finite Amplitude Ultrasonic Waves in Liquids," Phys. Fluids, V. 3, P. 346-352, 1960.

9. Weston, D. E., Proc. Phys. Soc., (London) B66, P. 695-609, 1953.

10. Ruff, P. G., Finite Amplitude Standing Waves in Rigid Walled Cavities, Thesis, Naval Postgraduate School, Monterey, California, 1967. R845

11. Coppens, A. B., "Theoretical Study of Finite-Amplitude Traveling Waves in Rigid-Walled Ducts: Behavior for Strengths Precluding Shock Formation." J. Acoust. Soc. Am., V. 49, P. 306-318, 1969.

12. Beech, W. L., Finite-Amplitude Standing Waves in Rigid-Walled Tubes, Thesis, Naval Postgraduate School, Monterey, California, 1967.

13. Winn, J. R., Fourier Analysis of Experimental Finite-Amplitude Standing Waves, Thesis, Naval Postgraduate School, Monterey, California, 1971.

W Amp 5

INITIAL DISTRIBUTION LIST

		No. Copies
1.	Defense Documentation Center Cameron Station Alexandria, Virginia 22314	2
2.	Library, Code 0212 Naval Postgraduate School Monterey, California 93940	2
3.	Assoc. Professor James V. Sanders, Code 61Sd Department of Physics Naval Postgraduate School Monterey, California 93940	1
4.	Assoc. Professor Alan B. Coppens, Code 61Cz Department of Physics Naval Postgraduate School Monterey, California 93940	1
5.	Lt. Roger R. DeVall, USN 1284 Leahy Road Monterey, California 93940	1

REPORT DOCUMENTATION PAGE		READ INSTRUCTIONS BEFORE COMPLETING FORM
1. REPORT NUMBER	2. GOVT ACCESSION NO.	3. RECIPIENT'S CATALOG NUMBER
4. TITLE (and Subtitle) Finite-Amplitude Waves in Imperfect Cavities		5. TYPE OF REPORT & PERIOD COVERED Master's Thesis; December 1973 6. PERFORMING ORG. REPORT NUMBER
7. AUTHOR(s) Roger Ronald DeVall		8. CONTRACT OR GRANT NUMBER(s)
9. PERFORMING ORGANIZATION NAME AND ADDRESS Naval Postgraduate School Monterey, California 93940		10. PROGRAM ELEMENT, PROJECT, TASK AREA & WORK UNIT NUMBERS
11. CONTROLLING OFFICE NAME AND ADDRESS Naval Postgraduate School Monterey, California 93940		12. REPORT DATE December 1973 13. NUMBER OF PAGES 62
14. MONITORING AGENCY NAME & ADDRESS(if different from Controlling Office) Naval Postgraduate School Monterey, California 93940		15. SECURITY CLASS. (of this report) Unclassified 15a. DECLASSIFICATION/DOWNGRADING SCHEDULE

16. DISTRIBUTION STATEMENT (of this Report)

Approved for public release; distribution unlimited.

17. DISTRIBUTION STATEMENT (of the abstract entered in Block 20, if different from Report)

18. SUPPLEMENTARY NOTES

19. KEY WORDS (Continue on reverse side if necessary and identify by block number)

Finite-Amplitude Standing Wave
Rigid-Walled Cavity
Strength Parameter
Frequency Parameter

20. ABSTRACT (Continue on reverse side if necessary and identify by block number)

Finite-amplitude standing waves in air at ambient temperatures contained within a detunable, rigid-walled rectangular cavity were experimentally investigated. The pressure waveforms resulting from excitations in the vicinity of the resonances of the 100 and 010 modes were analyzed for harmonic content at three different cavity configurations. Similarly,

waveforms of the 110 and 210 modes were analyzed for four different cavity configurations. These results were compared to the predictions of a theory of Coppens and Sanders wherein the resonance frequencies and quality factors of all modes were experimentally determined from infinitesimal-amplitude measurements. It was found that in the case of nearly degenerate modes, coupling within the cavity allowed for the excitation of modes belonging to families other than that containing the driven mode. This feature is absent from the theory in its present form.